An Analysis of the Red Giant Bump

Auteur : De Becker, Alexandre
Promoteur(s) : Dupret, Marc-Antoine; Grotsch, Arlette
Faculté : Faculté des Sciences
Diplôme : Master en sciences spatiales, à finalité approfondie
Année académique : 2019-2020
URI/URL : http://hdl.handle.net/2268.2/10028

University of Liège
Faculty of Sciences
Department of Astrophysics, Geophysics and Oceanography

An Analysis of the Red Giant Bump

presented by Alexandre de Becker

Under the supervision of
Prof. Marc-Antoine Dupret and Prof. Arlette Noels

A thesis presented for the degree of Master in Space Sciences

Academic year 2019/2020

Remerciements

J'aimerais remercier mes promoteurs, Arlette Noels et Marc-Antoine Dupret, pour m'avoir permis de travailler sur ce sujet des plus intéressants, ainsi que pour leur disponibilité et toute leur aide apportée tout au long de l'année, me permettant ainsi d'aboutir à ce résultat final.

J'aimerais également remercier mes parents grâce à qui j'ai réalisé les études qui me plaisaient et dont ce travail représente l'aboutissement, ainsi que toute ma famille pour son soutient tout au long de ces années et de ce travail.

Je remercie aussi mes amis pour leurs encouragements et les chouettes pauses qui permettaient de se remettre d'autant mieux au travail.

Enfin j'aimerais remercier Jeff, Douraya, Razvan et tout particulièrement Hélène pour le temps qu'ils ont pris pour lire mon travail et ainsi pouvoir me donner quelques conseils pour en améliorer sa rédaction.

Abstract

The red giant branch bump is a phenomenon that consists of a decrease in luminosity for a given time during the red giant branch phase and has been known for some time. Nevertheless, discrepancies between models and observations show that it is not yet fully understood. It is therefore interesting to try to understand the influence of various parameters that are part of the structure of the star on the bump. We have used the stellar evolution code called Clés to study the influence of the total mass of the star, its overshooting parameter, its undershooting parameter, its metallicity, and the microscopic and turbulent diffusion. To study the effects of changing these parameters, the attention was given to the track of the star in the Hertzsprung-Russell diagram during its evolution and on the hydrogen abundance profile of the star, the discontinuity in the latter being the key element for the appearance of the bump. Effects can be seen on the bump for each of the parameters studied, which can be summarized in two categories: a change in the luminosity at which the bump occurs and a change in the size of the bump, thus the importance of the observed decrease in luminosity.

Contents

1 Introduction

The red giant branch bump is a phenomenon known theoretically since the end of the sixties (Thomas 1967; Iben 1968) and then confirmed by observations during the eighties (King et al, 1985). Since then, a large number of much more recent works have been devoted to the red giant branch bump (Cassisi et al., 2001; Bjork and Chaboyer, 2005; Cassisi et al., 2011; Joyce and Chaboyer, 2015; Lagioia et al, 2015; Bossini et al., 2015; Khan et al. 2018; ...). In addition to being a current research topic, what makes it all the more interesting is the fact that there is a disagreement between models and observations. A deeper understanding of this phenomenon and the parameters which play a role in it may allow to obtain new constraints on errors and thus improve the theoretical models at our disposal. But what is this red giant bump?

Through its life, a star evolves. After the formation of the star and the descent on the hayashi track, where a global contraction leads to a heating of all the stellar layers, the star spends about 80 to 90 % of its lifetime on the so-called main sequence, during which hydrogen is transformed into helium in the central layers. Once it leaves the main sequence, it begins its ascension on the red giant branch (RGB) where its luminosity increases. For low mass stars, this ascension is momentarily reversed, their luminosity decreases before resuming their way up on the red giant branch. This temporary drop of luminosity is what we call the red giant branch bump.

But why is it called like that? Let's imagine that we observe a cluster of stars. As usual for clusters, it is assumed that all the members of the cluster have common properties, in particular, same age and same metallicity. Knowing this, a big amount of those stars have more or less the same evolution. For the low mass stars composing this cluster, the bump then happens more or less at the same luminosity. Each star has three times the luminosities contained in the range of luminosities of the bump. Therefore, there are some luminosities more probable to be observed than others. If a histogram of the number of stars per luminosity is drawn, a bump is observed at the concerned luminosities. Due to a passage on the same luminosity range three times during this phase of evolution, when a cluster is observed, there are more stars with typical luminosity of the bump.

My work for this master thesis consisted in analysing this bump. I had to run models of stellar evolution, modifying some physical properties to have a better understanding of the influence of those diverse parameters on the red giant branch bump.

Section 2 recalls the structural equations and other relationships that will be useful in understanding the phenomena outlined below and used by our stellar evolution code, which is also briefly described in this section.

As explained above, the bump takes place during the red giant branch phase. But the evolution that the star undergoes before reaching the RGB will have an impact on the bump. Section 3 then presents the evolution of the star from its formation until it reaches the RGB.

Section 4 describes what happens during the rise of the star on the red giant branch and why the bump occurs during this phase.

Section 5 is the heart of this master thesis. It presents the different parameters studied by showing the impact that a variation of these parameters implies on the bump and an explanation of what is observed is given from the hydrogen abundance profile in the star.

Section 6 provides a comparison of the results obtained with three papers on the bump read at the beginning of the work on this thesis.

Section 7 serves as a summary and conclusion to this master thesis.

2 Internal structure equations

To describe the internal structure of a star and the phenomena occurring in it, several equations are needed. These are presented below. Those equations allow to have a good understanding of what happens in the star and how it evolves throughout its life via the changes of the involved parameters.

2.1 Internal structure differential equations

Among the equations describing the interior of the star, four of them allow to describe the structure itself of the star. Those four equations are differential equations and may be expressed following two different variables, namely the mass and the distance to the center. Here, these equations are expressed as a function of mass because it will be the main landmark through this master thesis. Nevertheless, from those relations, their expressions according to the distance to the center can be easily found.

2.1.1 Mass conservation equation

The mass conservation equation gives a relationship between the mass inside a sphere of radius r and the radius via the density. With this equation, the mass for a given radius, or inversely the radius for a given mass, can be obtained:

$$\frac{dr}{dm} = \frac{1}{4\pi\rho r^2} \tag{1}$$

with r the distance to the center, m the mass contained in the sphere of radius r and ρ the density.

2.1.2 Hydrostatic equilibrium

The hydrostatic equilibrium is reached when the gravitational force and the force due to the pressure gradient compensate each other exactly, then:

$$\frac{dP}{dm} = -\frac{Gm}{4\pi r^4} \tag{2}$$

with P the pressure and G the universal constant of gravitation

2.1.3 The energy transfer

The temperature in the star is not uniform, which implies the presence of a temperature gradient. This temperature gradient induces a transfer of energy. In a star, the energy is globally transferred from the inside to the outside. There are two ways for this energy to be transported: by a radiative transfer of energy or by convective motions of matter. Depending on the part of the star and the stage of evolution of the star we are looking at, the zone under consideration can be radiative or convective. In either case, there is alway at least some part of the energy transferred by radiation.

The radiative transfer is written:

$$\frac{dT}{dm} = -\frac{3\kappa L}{64\pi^2 acr^4 T^3} \tag{3}$$

where T is the temperature, κ the opacity, L the luminosity, a the radiation density and c the speed of light.

In the case where the convection is effective:

$$\frac{dT}{dm} = -\nabla_{ad}\frac{Gm}{4\pi r^4}\frac{T}{P} \tag{4}$$

where ∇_{ad} is the adiabatic temperature gradient.

The Schwarzschild criterion is used to determine whether convection is effective or not. This criterion states that convection occurs if the radiative temperature gradient is greater than the adiabatic temperature gradient:

$$\nabla_{rad} > \nabla_{ad} \tag{5}$$

The radiative temperature gradient is given by:

$$\nabla_{rad} \equiv \frac{3\kappa PL}{16\pi acGmT^4} \tag{6}$$

This radiative temperature gradient is the value that the real temperature gradient should have so that all the energy would be transported by radiation.

The adiabatic temperature gradient is given by:

$$\nabla_{ad} \equiv \frac{\partial lnT}{\partial lnP}|_s \tag{7}$$

with s the entropy. It is thus the temperature gradient taken for a constant entropy. For an ideal gas, $\nabla_{ad} = 2/5$.

In convective regions, mixing is assumed to be instantaneous, which means that the chemical composition is constant all along the convective layers.

2.1.4 Conservation of energy

There are two possible sources of energy, one coming from the gravitational contraction, the other from nuclear reactions.

$$\frac{dL}{dm} = \epsilon_n + \epsilon_{grav} \tag{8}$$

where L is the total amount of energy produced per second in the sphere of radius r and mass m, ϵ_n being the production of energy due to nuclear reactions and ϵ_{grav} being the energy produced or absorbed due to the gravitational contraction or expansion.

The term ϵ_{grav} is generally very small when most of the energy is produced by nuclear reactions like during core hydrogen burning phases. It is however important to follow its evolution since it is the signature of stellar

readjustment to new physical conditions.

In the case where ϵ_{grav} is negligible, the star is in thermal equilibrium and the energy is considered as coming exclusively from the nuclear reaction. In thermal equilibrium the previous equation is written:

$$\frac{dL}{dm} = \epsilon_n \tag{9}$$

2.2 Constitutive equations

There are thus four differential equations to describe the internal structure of a star, $\frac{dr}{dm}$, $\frac{dP}{dm}$, $\frac{dT}{dm}$ and $\frac{dL}{dm}$, but also seven unknowns: r, ρ, P, T, L, κ and ϵ. Additional relations connecting these variables are therefore required.

2.2.1 Equation of state

The pressure inside a star may be considered as a sum of two components, the gas pressure and the radiative pressure:

$$P = P_g + P_{rad} \tag{10}$$

with P_g the gas pressure and P_{rad} the radiative pressure. The second term, P_{rad} is mostly relevant for high temperature stars so high mass stars. In low mass stars, this term may be neglected and only the gas pressure is considered. This last can be given by the equation of state.

For the equation of state, two cases can be distinguished. The first one is when we may assume we have a non-degenerate ideal gas described by the Maxwell-Boltzmann distribution, the second case is when we have a degeneracy of the gas of electrons obeying a Fermi-Dirac distribution.

For a non-degenerate gas:

$$P_g \simeq \frac{k\rho T}{\mu m_u} \tag{11}$$

where k is the Boltzmann constant, μ is the mean molecular weight which is the mean mass of stellar particles and m_u is the atomic mass constant.

For the degenerate case, it can again be subdivided in two different cases, whether the gas is relativistic or not.
In the non-relativistic case:

$$P_e \simeq K_1 \rho^{\frac{5}{3}} \tag{12}$$

and in the relativistic case:

$$P_e \simeq K_2 \rho^{\frac{4}{3}} \tag{13}$$

P_e is the pressure of the gas of electrons, K_1 and K_2 are constants with $K_1 = \frac{8\pi}{15h^3 m_e}(\frac{3h^3}{8\pi m_u})^{\frac{5}{3}}$ and $K_2 = \frac{2\pi c}{3h^3}(\frac{3h^3}{8m_u})^{\frac{4}{3}}$

2.2.2 Energy production

As seen in the conservation of energy equation, the energy may be produced via two different processes, the gravitational contraction and the nuclear reactions.

The energy production by gravitational contraction ϵ_{grav} is written:

$$\epsilon_{grav} = \frac{du}{dt} + P\frac{dv}{dt} \tag{14}$$

With u the internal energy, t the time and v the specific volume. It takes into account the variation of internal energy and the work done by the gravitational contraction.

The energy production by nuclear reaction ϵ_n depends on which nuclear reaction is happening. In the context of the study of the red giant branch bump, the only relevant nuclear reaction is the hydrogen combustion. Therefore, attention is focused on this one. There are however still two different cases. Indeed, there are two ways to produce helium from hydrogen, via the pp chain or via the CNO cycle. The production of energy via those two processes can be written:

$$\epsilon_{pp} \sim C_{pp} X^2 \rho T^5 \tag{15}$$

for the pp chain, and

$$\epsilon_{CNO} \sim C_{CNO} X_{CNO} X \rho T^{15} \tag{16}$$

for the CNO cycle.
In those equations, C is a constant, different for the pp chain and the CNO cycle, X is the abundance of hydrogen and X_{CNO} is the abundance of carbon, nitrogen and oxygen taken together.

Because of the greater temperature sensitivity of CNO reactions, it is obvious that this way of producing helium will be favoured when the temperature is increased.

2.2.3 Opacity

The opacity is a factor linked to the interaction between matter and radiation. The higher the opacity, the more interactions there is. Then, the higher the opacity, the lower the chance of a photon traveling freely through the stellar layers. A high opacity "blocks" the photon, thus also the transfer of energy through radiation.

The Kramers' law provides an approximate relation for the opacity, due to bound-free and free-free atomic transitions mainly responsible for the opacity in low mass stars. This law is written:

$$\kappa = C f(X, Y, Z)(1 + X) \rho T^{-3.5} \tag{17}$$

where κ is the opacity, C a constant and f(X,Y,Z) a term depending on the chemical composition, Y being the helium abundance and Z the metallicity.

It shows that opacity increases with decreasing temperature, which is the reason why convection is present in the outer layers of low-mass stars.

2.3 Stellar evolution code

In order to modelize the different stars studied in this work, we use the stellar evolution code Clés which stands for *Code Liégeois d'Évolution Stellaire* (Scuflaire et al., 2007), developed by the Department of Astrophysics and Geophysics of Liège.
This code allows to model a star for which certain parameters are set and to follow its evolution during its life. To achieve this, the code uses the equations of structure and the constitutive equations presented above in sections 2.1 and 2.2.
To use the code it is necessary to use some external data such as for nuclear reactions, equations of state or opacity. For nuclear reactions we refer to *"Solar fusion cross sections. II. The pp chain and CNO cycles. Reviews of Modern Physics"* (Adelberger et al. 2011). For state equations we use the code *"FreeEOS: Equation of State for stellar interiors calculations"* (Irwin, 2012). For the opacity, the data are taken from *"OPAL Equation-of-State Tables for Astrophysical Applications"* (Rogers et al., 1996).

3 From the formation to the Red Giant Branch

Let's begin by a quick review of the evolution of a star, from its formation until it reaches the red giant branch and the bump.

3.1 Pre main sequence

The formation of a star begins when a perturbation inside a molecular cloud induces the contraction of a part of this molecular cloud. We can consider that the star is born once the contracting material reaches the hydrostatic equilibrium. At this point, there is not yet nuclear energy production since the temperature inside the star is too small, all the energy comes from the contraction of the star which continues even if it has been slowed down when reaching hydrostatic equilibrium. This phase is called the Hayashi phase and is represented as an almost vertical line on the Hertzsprung-Russell diagram (HR diagram), which relates the logarithm of the stellar luminosity and the logarithm of the effective temperature. The effective temperature is thus almost constant while the luminosity is decreasing. During this phase, the star is completely convective.

After this descent on the Hayashi track, depending on the mass of our star, the onset of the nuclear reactions occurs or not. The bump concerns low mass stars but not too low. Indeed, as it will be shown later, the bump happens during the red giant branch phase following the main sequence and to reach those phases, the fusion of hydrogen must occur inside the star.

Since the hydrostatic equilibrium is established, the Viriel theorem for a non-relativistic monoatomic ideal gas sphere writes:

$$E_g = -2E_i \tag{18}$$

with E_g the total gravitational potential of the star and E_i its internal energy.
The star contracts, releasing potential energy. The Viriel theorem tells us that half of this released energy is converted into internal energy while the rest is radiated. Since the internal energy is proportional to P/ρ, this increase

of internal energy leads to an increase or a decrease of the temperature depending whether the star is degenerate or not.

For too low mass stars, the limit being approximately at 0.08 $M_\odot$, due to the degeneracy of the electrons, temperatures reach a maximum before they drop and are never high enough to trigger hydrogen fusion. Those stars are the so-called brown dwarfs. The temperature of the brown dwarfs then continues to decrease with time. The onset of the nuclear reactions may begin when the central temperature neighbors 10^7 K and this required temperature is never reached in in the brown dwarfs case.

For more massive stars, the contraction of the star results in an increase of the temperature. This increase of the temperature leads to a decrease in the opacity, see equation (17), and this decrease of opacity leads to a decrease of the radiative temperature gradient. Following the Schwarzschild criterion (equation (5)), a radiative core appears. After some time, the core temperature reaches a sufficiently high value to onset the burning of the hydrogen. With the onset of nuclear reactions, a restructuring of the interior of the star occurs and a slight decrease in luminosity and effective temperature is observed.

To follow the evolution of the star, let's take a closer look at the hydrogen abundance. In what follows, the same star, with a mass of 1.3 $M_\odot$, is considered at each stage of its evolution.

During the pre main sequence, the hydrogen abundance profile is as shown in blue in Figure 1. Since there are no nuclear reactions yet, it is normal to observe that it is constant over the whole star.

3.2 Main sequence

3.2.1 Nuclear energy

After stabilization the star reaches the ZAMS, the Zero Age Main Sequence, which is simply the beginning of the main sequence. Thermal equilibrium is reached, all the energy comes then from the nuclear reactions, and the hydrodynamic equilibrium is still present.

When the star reaches the ZAMS, the hydrogen burning in the core starts. This leads to a variation of chemical composition, the mean molecular weight increases and this change is now the element responsible for the evolution of the star during the main sequence phase. The stars spend the biggest part of their life in the main sequence. This time spent in the main sequence depends on the mass of the star. Indeed, it can be shown that the luminosity is proportional to the mass.

$$L \propto M^{\alpha}$$

The exponent α will depend on the mass but is of the order of three for low and intermediate mass stars and close to one for massive stars. From this, it can be observed that the luminosity is higher for more massive stars. A higher luminosity means that the star has a higher nuclear energy production, the hydrogen is then consumed faster and the star spends less time in the main sequence.

3.2.2 Convective core

During this phase, the stars may have a convective core or not. As it will be shown later, the presence of a convective core during the main sequence influences the bump. The occurrence of convection is linked to the type of nuclear reactions present for the hydrogen burning, and this in turn depends on the mass of the star. Below a mass limit of about 1.2 $M_{\odot}$, the hydrogen burning occurs through pp chains reactions and the core is radiative. Above the limit of 1.2 $M_{\odot}$, the helium is formed through CNO cycle and the star has a convective core. The production of energy via those two processes is given by equations (15) and (16).

From equation (6), a high L/m ratio leads to a high radiative temperature gradient. Thanks to the Schwarzschild criterion (equation (5)) we know it favors a convective transport of the energy. By expressing the luminosity from the equation of conservation of the energy (equation (8)) taking into account the thermal equilibrium and using equations (15) and (16), we have:

$$L = \int_0^M \epsilon_{pp/CNO} dm \sim \int_0^M \rho T^\nu dm \tag{19}$$

With ν the temperature sensitivity, which is of the order of 5 for the pp chain and 15 for the CNO cycle as see in equations (15) and (16). The ratio L/m is thus proportional to T^ν. This higher sensitivity to the temperature of the CNO cycle explains thus a higher ratio L/m and thus the appearance of convection in the core of the star, when helium is produced this way, which happens in stars more massive than about 1.2 $M_\odot$.

3.2.3 Overshooting-Undershooting

As stated previously, the fact that there is or not a convective core is important for the study of the red giant branch bump. When the core is convective, the matter moves up and down in it. It happens that matter goes beyond the limit of the convective core. This is what is called overshooting. The mass extent of the overshooting region as well as the efficiency of the mixing are still unknown. For its extent it is generally assume that overshooting takes place over a distance l given by:

$$l = \alpha H_P \tag{20}$$

where α is the overshooting parameter, of the order of a few tenths and H_P is the pressure scale height at the convective core boundary. The overshooting parameter is one of the most troublesome uncertainties in stellar evolution modeling.

Moreover it is generally assume that in the overshooting region above the convective core, a full mixing occurs instantaneously, as it is the case in the convective core itself. This means that overshooting has the primary effect of increasing the mass of the fully mixed material in stars. The overshooting thus modifies the profile of the abundance of hydrogen which, as will be seen later, is the key element of the bump.

Since low mass stars have a convective envelope (see Section 2.2.3), just like overshooting may happen in a convective core, some undershooting can

also occur below the lower boundary, adding another uncertainty to the stellar modeling. The phenomenon occurs the same way as the overshooting: matter moves up and down in the convective envelope and some matter goes beyond its limit, reaching then deeper layers.
For the undershooting a parameter α is also used, this time called undershooting parameter and the pressure scale height H_p is taken at the base of the envelope.

3.2.4 Diffusion

Some processes happen on a small scale, like it is the case of the microscopic diffusion. It results from two processes: the gravitational settling and the radiative forces. The first one, linked to the gravitational force, brings down the heavier elements while the lighter elements are brought upwards. The radiative force pushes up particles with high cross-section while particles with low cross-section go down.

The speed of diffusion depends on the depth in the star. It will be fast at the surface but slow in the deep layers of the star.

As heavy elements fall down as a result of diffusion, they reach the boundary of the convective core where they increase the opacity and favor a slightly larger convective core. The diffusion will then, as the overshooting, modifies the hydrogen profile and thus also what happens during the bump.

In addition, levitation of ionized matter occurs as a result of radiative accelerations and can somewhat counterbalance the effects of microscopic diffusion. This induces another uncertainty in the chemical profiles since it is absent in most stellar evolution codes, in particular in Clés.

3.2.5 Global evolution

During the evolution in the main sequence, the star undergoes a contraction of its core, where nuclear reactions take place, and an expansion of its envelope, i.e. the layers located above the core. Globally, the radius of the star increases. The contraction of the core results from the transformation of hydrogen into helium, leading to an increase in the mean molecular weight in the affected regions. The equation of state (11) shows that pres-

sure, temperature, density and mean molecular weight are all linked together. The change of the mean molecular weight thus impacts the other physical properties. Temperature is however kept quasi constant through a process generally called the "pressure thermostatic control mechanism" that will not be described here.

Regarding the luminosity of the star, it has been stated just above that there are two kinds of nuclear processes. The luminosity increases more in the case where there are pp chain reactions than in the case of CNO cycle reactions, where the luminosity is even almost constant.

Finally the effective temperature remains constant when the pp chain is responsible for the reactions, while it decreases in the case of CNO cycle reactions.

3.2.6 Hydrogen profile

Figure 1 shows in purple the hydrogen abundance profile as a function of the fractional mass q=m/M during the main sequence of a 1.3 $M_{\odot}$ star. There are several profiles in order to be able to follow the evolution of this one during the main sequence. The profile during the pre main sequence is also shown in blue and the one during the post main sequence in red:

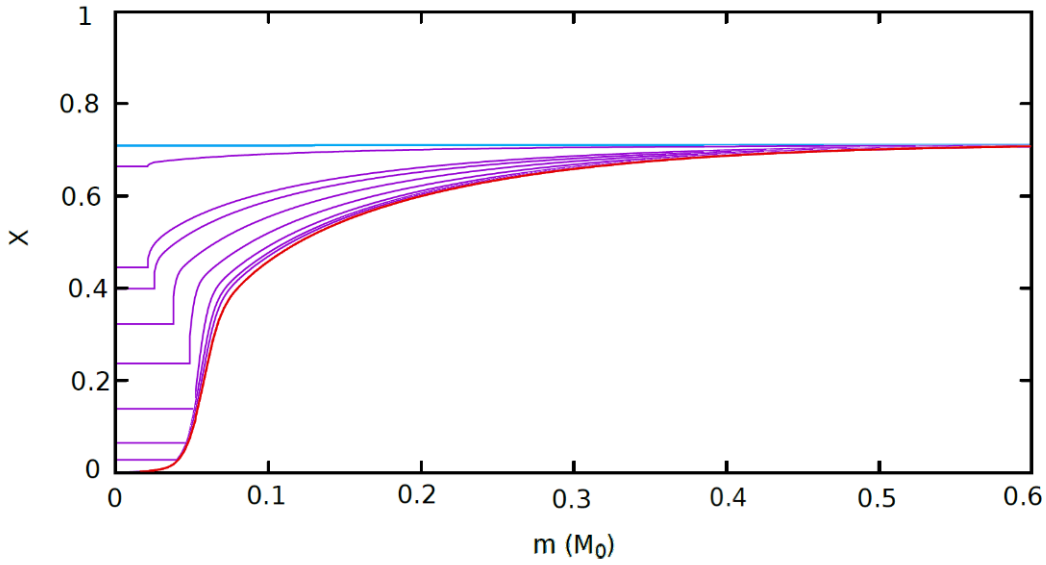

Figure 1: X profile as a function of the fractional mass q=m/M during the pre main sequence (blue), main sequence (purple) and post main sequence (red) of a $1.3 M_{\odot}$.

On this profile, the effect of the onset of nuclear reactions can easily be noted. The initially uniform hydrogen abundance is no longer homogeneous. During the main sequence, the hydrogen is consumed in the core and there is less and less hydrogen in it. Since the star is beyond the limit of 1.2 $M_{\odot}$, the hydrogen combustion takes place here via the CNO cycle and therefore a convective core is present. The convective core can be seen as the plateau at the core of the star in the profiles shown above. During the main sequence, it first expands and then becomes smaller again. Even if the convective core is considered to be the plateau, the abundance of hydrogen also decreases beyond it. Nuclear reactions therefore also take place beyond the convective core. As the mass of the convective core decreases, the area where nuclear reactions take place shrinks and the core leaves behind a gradient of hydrogen abundance. As the hydrogen abundance is constant beyond 0.6 $M_{\odot}$ the profiles are only shown up to this point in order to highlight the profiles behavior close to the center.

3.3 Post main sequence

After all the hydrogen has been consumed in the core of the star, it remains a core composed of helium which is devoid of energy source since the temperature is too small to start transforming helium into carbon and oxygen. This helium core is thus isothermal. Around this isothermal helium core, there is a hydrogen burning shell which will add more and more helium to the core. But the isothermal helium core have a mass limit beyond which it can't support the envelope mass. This limit is called the Schönberg-Chandrasekhar mass limit and may be written:

$$\frac{M_c}{M} = 0.37(\frac{\mu_{env}}{\mu_{core}})^2 \tag{21}$$

Where M_c is the mass of the isothermal helium core, M the total mass of the star, μ_{env} is the mean molecular weight of the envelope and finally μ_{core} is the mean molecular weight of the core.

This mass limit comes from the fact that the pressure at the isothermal core border does not increase continuously with the mass of the core. It reaches a maximum above which the core cannot hold anymore the pressure of the envelope. The core will then contract and will eventually become degenerate while the envelope is still expanding. The star undergoes a thermal runaway which leads to a lower and lower effective temperature and an evolution towards the red giant branch located in the area of the Hayashi track. This phase is quite fast and stabilization occurs when the star reaches the red giant branch, with an extended convective envelope.

Resulting from the energy released by the contraction of the core, a temperature gradient forms in the so far isothermal layers. However as the density increases and the matter becomes more and more degenerate, electron conduction becomes the dominant contributor to the energy transfer and this translates in a lower and lower opacity. Equation 8 shows that the radiative temperature gradient becomes lower and lower, i.e. a quasi isothermal core is formed afresh.

The hydrogen abundance profile in the post main sequence can be seen in figure 1 in red. On this profile it can be seen that the core has absolutely no

hydrogen left, all of it has been consumed. As previously stated, the helium core is isothermal, so there is no convection.

To be noted, only low mass stars will reach this Schönberg-Chandrasekhar limit after completing core hydrogen burning and have a degenerate core before beginning their ascension on the red giant branch. More massive stars end their main sequence with a helium core already larger than the Schönberg-Chandrasekhar limit.

Figure 2 shows the HR diagram for a 1.3 $M_\odot$ on which we see the different part of the evolution discussed above. We have the Hayashi track in 1, the "radiative" pre main sequence in 2, also called the Henyey track, the main sequence in 3 and the transition between the main sequence and the red giant branch in 4. The next phase, the red giant branch, is shown in 5.

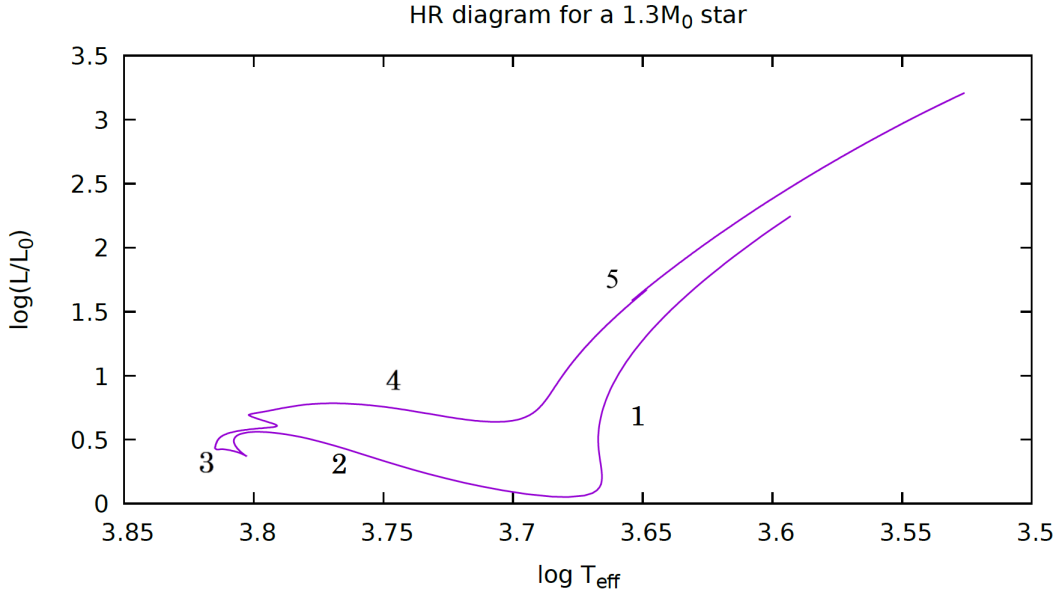

Figure 2: HR diagram for a 1.3 $M_\odot$ on which we see the different part of the evolution we discussed above. 1: The Hayashi track; 2:Pre main-sequence (Henyey track); 3: The main sequence; 4:The transition between the main sequence and the red giant branch; 5: The red giant branch

4 The Red Giant Branch and the bump

4.1 The red giant branch

During its life on the red giant branch, the star structure is "divided" into 4 parts. The first one at the center, is an isothermal, degenerate helium core. Above the core, there is a shell in which CNO reactions transform hydrogen into helium. At the surface of the star, there is a convective envelope. Finally, the last part is a radiative zone located between the shell and the envelope, which becomes thinner and thinner as the convective envelope extends and reaches deeper and deeper layers.

As hydrogen is transformed into helium in the shell, the mass of the helium core increases and the shell moves outward toward fresher hydrogen layers. During this phase, a contraction of the core and an expansion of the envelope occur. This expansion of the envelope leads to a decrease of the temperature and according to the Kramers' law (equation 17) an increase in the opacity happens. The higher opacity leads to a higher radiative temperature gradient. According to the Schwarzschild criterion, the envelop goes thus deeper in the star.

At the onset of the RGB phase, the envelope has a chemical composition still very close to the initial composition since convective mixing dilutes the chemical impact of diffusion. As it goes deeper, in the region where the chemical composition was affected by nuclear burning during main sequence, a mixing of chemically inhomogeneous matter occurs. This mixing brings some material towards the surface, like for example the ^{14}N much more abundant in CNO affected regions, this is called the first dredge-up. The convective envelope is fully mixed and when it reaches layers left by the receding convective core during the main sequence, a discontinuity in chemical composition is formed just at the lower boundary of the envelope. However, as the shell moves outward as a result of hydrogen burning, the temperature increases below the convective envelope and the deepening of this envelope is reversed, leading to a chemical discontinuity located at the deepest level reached by the envelope.

What happens globally during the ascension on the red giant branch? As said previously, the core accumulates helium so its mass increases while its

radius decreases. From homology relations it can be shown that in a non degenerate matter that the temperature can be written:

$$T_{shell} \propto \mu_{shell} \frac{M_{core}}{R_{core}} \tag{22}$$

Where T_{shell} is the temperature in the H-burning shell, μ is the mean molecular weight in the shell, M_{core} is the mass of the isothermal helium core and R_{core} its radius.

As this relationship is important to understand the behavior of the star during the RGB phase and the bump, it is interesting to look at how we get it. Assuming, then, that homological relationships are valid for the expansion of the shell of our star, the following can be written:

$$T(r) = t(r/R_{core}) T_{core}(M_{core}, R_{core}) \tag{23}$$

and

$$P(r) = p(r/R_{core}) P_{core}(M_{core}, R_{core}) \tag{24}$$

where T(r) and P(r) are respectively the temperature and the pressure at a radius r. These two quantities are therefore expressed as the product of two functions, one dependent on r/R_{core}, $t(r/R_{core})$ for the temperature and $p(r/R_{core})$ for the pressure, and the second dependent on the mass and radius of the helium core, $T_{core}(M_{core}, R_{core})$ for the temperature and $P_{core}(M_{core}, R_{core})$for the pressure.

Using the integrated form of hydrostatic equilibrium, the pressure can be written as:

$$P(r) = P(r_0) - \int_{r_0}^{r} \frac{Gm\rho}{r^2} dr \tag{25}$$

with r_o being the distance between the center of the star and the top of the shell.

As the weight of the envelope is really low, it does not affect significantly the shell and the pressure at the top of the shell can therefore be neglected. The mass of the shell being negligible compared to that of the helium core,

the mass can be approximated as always being that of the core and can thus be taken out of the integral. Then:

$$P(r) \simeq -GM_{core} \int_{r_0}^{r} \frac{\rho}{r^2} dr \tag{26}$$

To obtain a relationship of the same form as equation 24, the change of variable $y = R_{core}/r$ is used, then:

$$P(r) \simeq \frac{GM_{core}}{R_{core}} \int_{y_o}^{y} \rho(y) dy \tag{27}$$

From the equation of state for a non-degenerate gas (equation 11), T(r) expressed and P(r) is replaced with its expression in equation 27:

$$T(r) = \frac{P(r)\mu m_u}{\rho k} = \frac{GM_{core}}{R_{core}} \frac{\int_{y_0}^{y} \rho(y) dy}{\rho} \frac{\mu m_u}{k} = t(r/R_{core})\mu \frac{M_{core}}{R_{core}} \tag{28}$$

r being taken in the shell, one obtains well the relation (22).

The increase of the mass and the decrease of the radius favor an increase of the temperature as long as a decrease in the mean molecular weight inside the shell does not reverse this temperature increase.

As for the luminosity, the following relation can be written:

$$L \propto \epsilon M_{shell} \propto \rho T_{shell}^{15} M_{shell} \tag{29}$$

Where L is the luminosity essentially produced inside the H-burning shell, ϵ is the nuclear energy rate and T_{shell} and M_{shell} are respectively the temperature and the mass of the shell.

The luminosity is proportional to the energy production by the nuclear reaction, itself proportional to the temperature. The conclusion is that the luminosity will increase with the temperature of the shell.

4.2 The bump

When the shell reaches the discontinuity left by the envelope, the hydrogen abundance suddenly increases, modifying at the same time the mean molecular weight. The hydrogen abundance is higher, so the mean molecular weight become smaller. As shown in equation (22) above, the temperature in the shell is directly linked to the mean molecular weight and, as μ decreases more than compensates the increase in $\frac{M_{core}}{R_{core}}$, the temperature also decreases. Since the luminosity is proportional to the temperature, it is easy to conclude that the decrease of the mean molecular mass leads to a decrease of the luminosity.

It is important to note that this decrease of luminosity happens only for a while when the discontinuity is reached by the shell. As said previously, the global behavior of the luminosity is an increasing along the RGB. The difference here with the "normal" situation, is that the change of mean molecular mass happens suddenly. In the normal situation, higher hydrogen abundance reached while the shell moves along the hydrogen profile, and therefore the decrease of the mean molecular weight, are always present, but are compensated by the increase in the factor $\frac{M_{core}}{R_{core}}$ in the equation (22). The discontinuity makes the change of μ too large and too fast to be compensated by $\frac{M_{core}}{R_{core}}$.

Since quasi all the energy production in the star comes from the shell, a decrease of luminosity in the shell means then a global decrease of the luminosity.

After the encounter of the chemical discontinuity, the hydrogen abundance becomes constant and as the $\frac{M_{core}}{R_{core}}$ term continues to increase, we then return to normal regime and the star continues its ascent on the red giant branch.

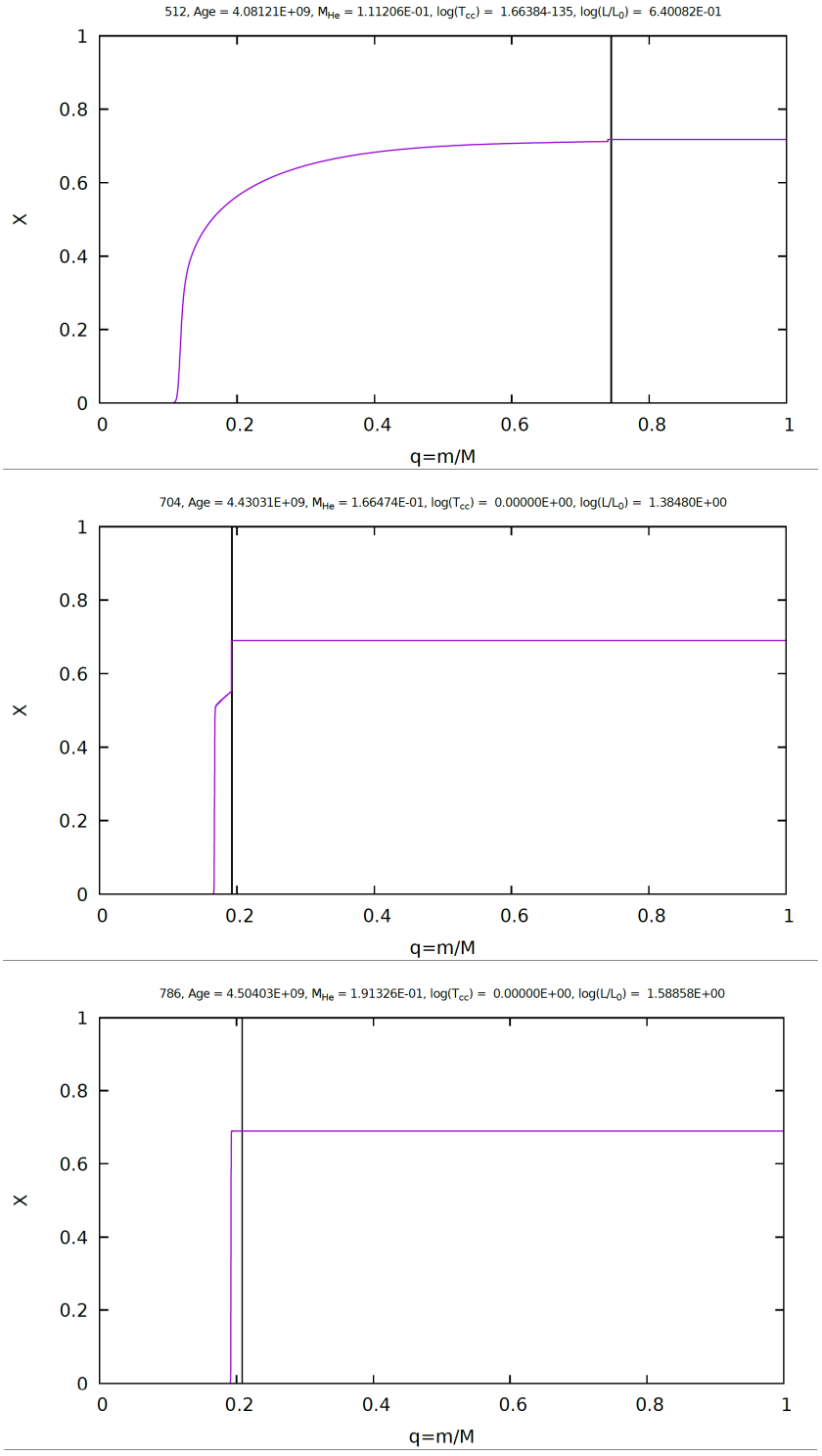

Figure 3: The profile of X for a $1.3 M_{\odot}$ star at three different moments. On the first graph when the base of the envelope, represented by the black vertical line, is still quite high, the second when the envelope reaches its maximum depth and the last when the H-burning shell reached the discontinuity.

Figure 3 shows the profile of X for a 1.3 $M_\odot$ star at three different moments on the red giant branch. The H-burning shell is located just above the helium core. On each profile, the base of the convective envelope is indicated by a vertical black line.
On the first profile, the base of the convective envelope is still far from the H-burning shell. This base of the envelope goes deeper with time. On the second profile, the base of the envelope at its maximum depth. The chemical discontinuity is clearly visible at a fractional mass of the order of 0.2. On the last profile, the H-burning shell has reached the chemical discontinuity, while the convective envelope recedes towards the surface. The H-burning shell moves now in layers with a constant chemical composition.

The end of the red giant branch evolution is marked by the onset of helium burning. Due to the fact that we have an isothermal fully degenerate helium core, the temperature of the core is approximately the same as the one of the shell. The equation (22) tells us that $T_{shell} \propto \frac{M_{core}}{R_{core}}$ so $T_{core} \propto \frac{M_{core}}{R_{core}}$ where T_{core} is the temperature of the core. A temperature approaching $10^8 K$ is required to begin the helium burning. For our low mass stars, whatever the total mass as long as the core is degenerate, this always happens when the helium core reaches 0.48 $M_\odot$.

4.3 High mass stars

For higher mass stars with partly degenerate or non degenerate helium core, the end of the red giant branch is also marked by the start of helium burning. However, the core temperature increases due to its contraction and it eventually reaches a temperature high enough to begin the helium burning before having a core mass of 0.48 $M_\odot$. This may happen before the encounter of the shell with the chemical discontinuity. As seen in the explanation of the red giant branch bump, the H-shell reaching the discontinuity is the key element for the occurrence of this phenomenon. In this case, there is then no bump during the red giant branch ascension.

Figure 4 shows the hydrogen profile in a 2.5 $M_\odot$ star. A yellow vertical line has been drawn to illustrate the boundary of the convective core due to core helium burning.

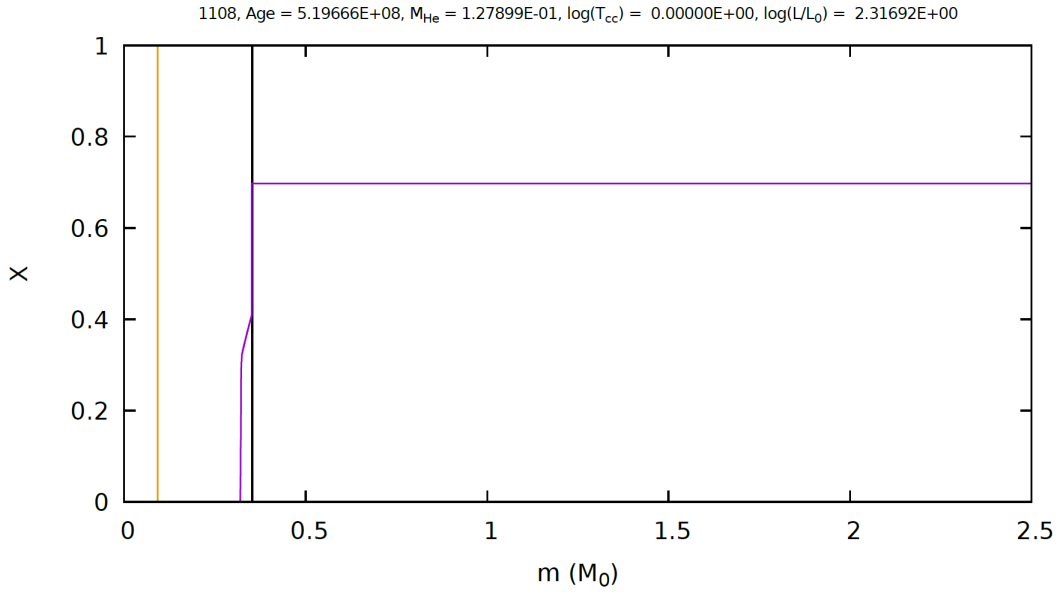

Figure 4: Profile of X for a 2.5 $M_{\odot}$ star at the end of the red chiant branch phase. The yellow line indicates the upper limit of the convective core due to core helium burning.

4.4 Energy production

One way to see the H-burning shell progressing through the star is to look at nuclear power generation.
Figure 5 shows energy production as a function of mass fraction. In purple is represented ϵ_{ν} which is the production of nuclear energy while in green is represented ϵ_{grav}, the energy coming from the contraction of the star.
Two information can easily be observed on this graph. The first is that there is no energy production due to the contraction during the red giant phase, or at least at a very negligible rate compared to nuclear power production. So we are well into thermal equilibrium. The second observable information is the peak that ϵ_{ν} is doing. It can be seen that all nuclear power generation is produced in a fairly thin region. That region is the H-burning shell. By observing the evolution of the position of this peak in the star, it is possible to follow the displacement of the shell.

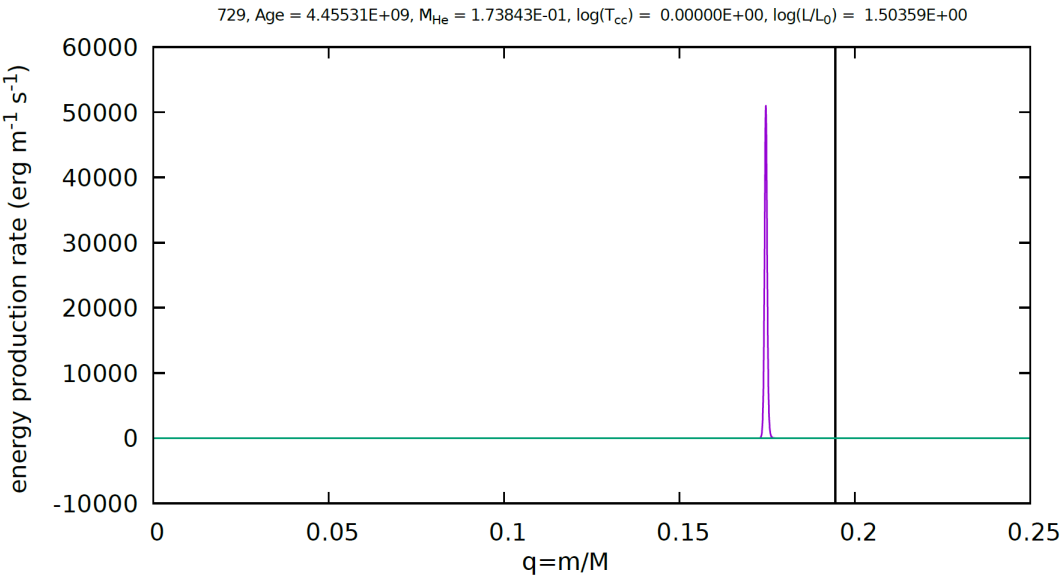

Figure 5: Energy production rate via the nuclear reactions (purple line) and via the gravitational contraction (green line) in function of the fractional mass q=m/M at a given moment during the red giant phase

4.5 Temperature gradients

Three different gradients can be distinguished: the radiative temperature gradient, the adiabatic temperature gradient and the real temperature gradient. The radiative and adiabatic temperature gradients are given by the equations (6) and (7) respectively. The real temperature gradient always has the value of one of the other two, whichever has the lower value.
Figure 6 shows a profile of these different gradients during the bump. In green can be seen the adiabatic temperature gradient, which is almost constant. In purple can be seen the radiative temperature gradient. In blue is represented the real temperature gradient which covers the radiative temperature gradient, and is therefore equal to it, to the left of the black vertical line and covers the adiabatic temperature gradient, and is therefore equal to it, to the right of this line. This black vertical line represents the boundary of the convective envelope. On the right side of this limit, the adiabatic temperature gradient is smaller than the radiative temperature gradient. According to

the Schwarzschild's criterion (5), there is a convective zone on this side, the envelope. On the left side, the radiative temperature gradient being smaller than the adiabatic temperature gradient, the same criterion shows well the presence of a radiative region. So, by looking at the evolution of these different gradients, it is possible to follow the evolution of the radiative region and the convective envelope and thus also the bump.

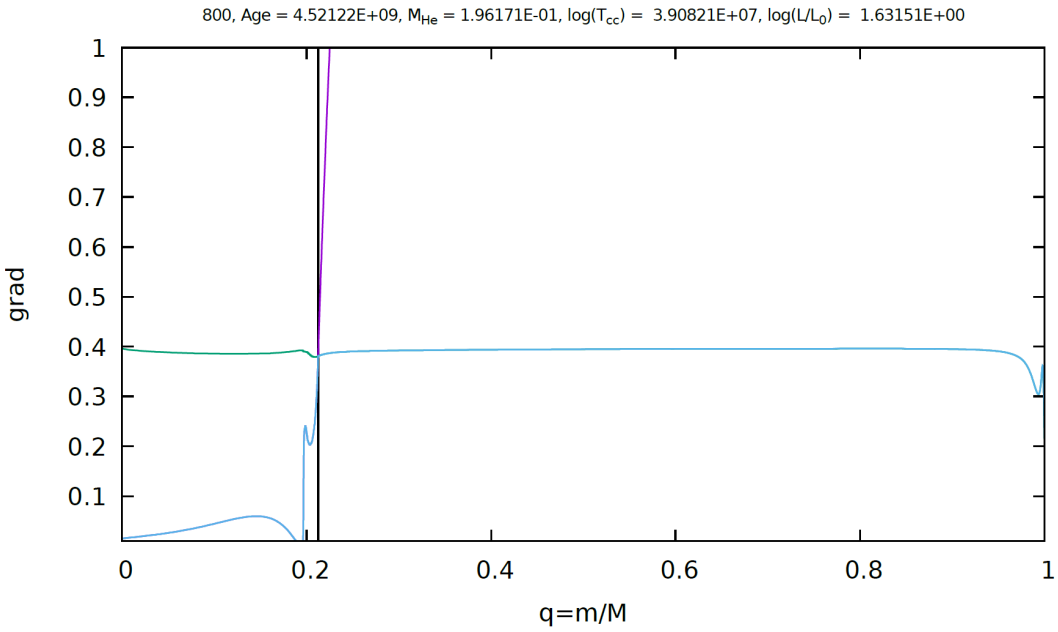

Figure 6: Radiative temperature gradient (purple), adiabatic temperature gradient (green) and real temperature gradient (blue) in function of the fractional mass q=m/M during the red giant phase

5 Study of the different parameters

Although the main mechanism for the appearance of the bump is understood, namely the encounter of the H-burning shell with the discontinuity of the hydrogen abundance, there is a discrepancy between the theoretical models and the observations. This discrepancy tells that this phenomenon is not yet fully understood, or, to use different terms, theoretical models are not yet perfectly developed. This is not surprising since, as already mentioned, uncertainties such as overshooting and diffusion affect the computation of stellar models.
One way to better understand the red giant branch bump is then to run evolutionary models with different sets of parameters. For this study, several models were run with the code Clés and the physics described in Section 2.3, changing various parameters to see how they affect the evolution of the star. More specifically, investigations were focused on their impact on the extent and location of the bump in the HR diagram. The hydrogen abundance profile in the star was then used to understand these effects.

The different parameters discussed in the following sections are the mass, the overshooting, the undershooting, the metallicity and finally the diffusion.

5.1 The mass

The total mass of a star is an important parameter. As shown in previous sections, it is crucial for the type of nuclear reactions during the main sequence and for the amount of electron degeneracy in the helium core during the ascension of the red giant branch.

The figure 7 shows the tracks in the HR diagram for four different masses. The first on is for a 1.0 $M_\odot$ star, the second one a 1.3 $M_\odot$ star, the third one a 1.8 $M_\odot$ star and finally a 2.2 $M_\odot$ star, respectively represented in purple, green, blue and yellow.

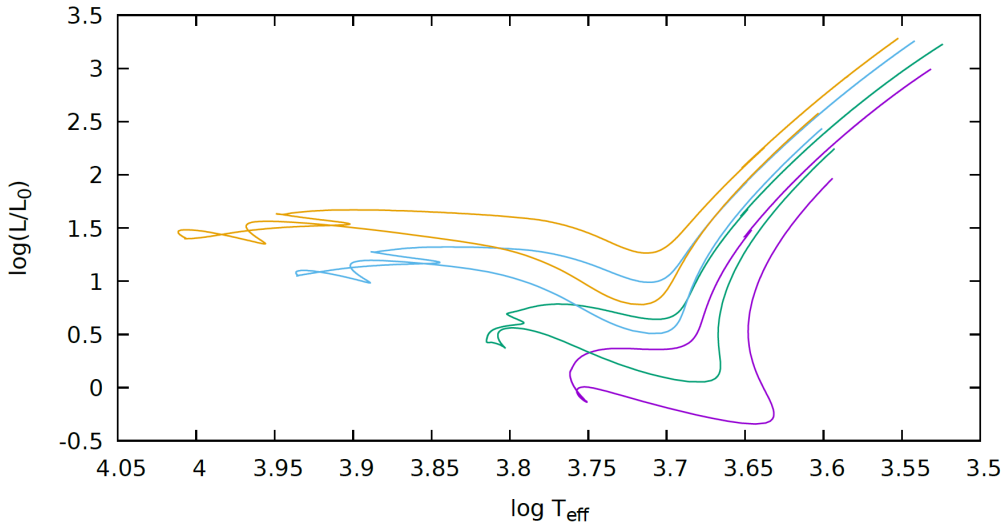

Figure 7: Tracks in the HR diagram for four stars having different masses: 1.0 $M_\odot$ (purple), 1.3 $M_\odot$ (blue), 1.8 $M_\odot$ (green) and 2.2 $M_\odot$ (yellow).

The overall shape of the different curves is globally the same but nevertheless with significant differences.
The first point is the general "translation" of the curves. For a same phase, a more massive star is more luminous and hotter than a less massive star.
A change in the behaviour of the curve can also be observed during the main sequence as the result of core hydrogen burning through pp or CNO reactions (see Section 3.2.5)
Finally a difference is observable during the bump. The figure 8 shows a zoom on this part of the evolution in the HR diagram:

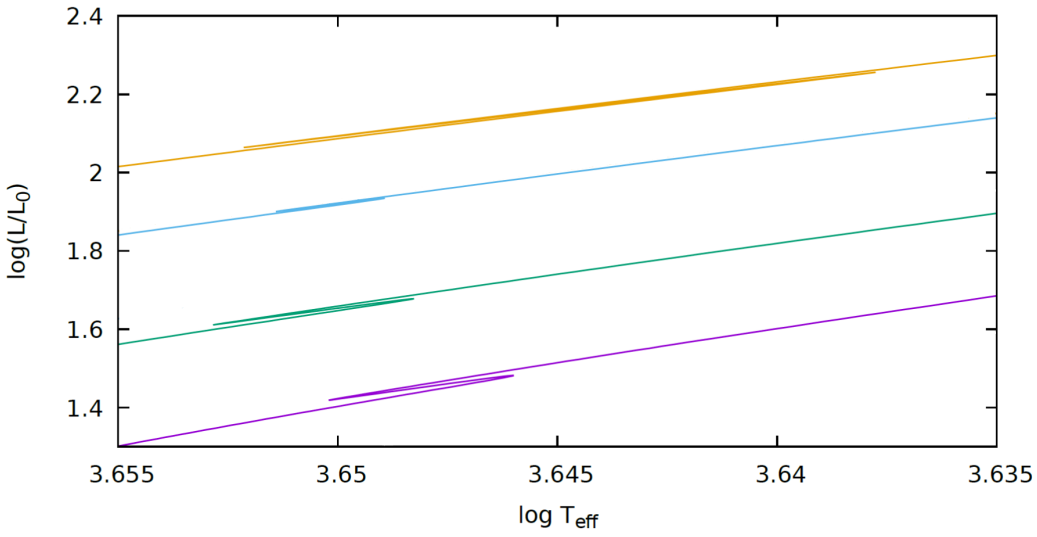

Figure 8: Tracks in the HR diagram, zoomed in on the bump part, for four stars having different masses: 1.0 $M_\odot$ (purple), 1.3 $M_\odot$ (blue), 1.8 $M_\odot$ (green) and 2.2 $M_\odot$ (yellow).

On this zoom, the bump for each mass considered is clearly identifiable. Each of these bumps differs from the others in two aspects.
The first aspect is the position in the HR diagram. This difference in position indicates that the bump does not occur at the same luminosity as a function of the mass of the star. The more massive the star is, the brighter it is when the bump starts. The beginning of the bump occurs at a luminosity of approximately $1.48L_\odot$, $1.66L_\odot$, $1.93_\odot$ and $2.25L_\odot$ respectively for masses of $1.0M_\odot$, $1.3M_\odot$, $1.8M_\odot$ and $2.2M_\odot$.
The second aspect is the size of the bump. It can be seen that the decrease in luminosity before it increases again can be more or less important depending on the mass of the star. An interesting point to note is that the size of the bump does not always evolve in the same way when looking at a higher (or lower) mass. For example, if the studied mass is increased from $1.3M_\odot$ to $1.8M_\odot$, the size of the bump decreases, whereas an increase to $2.2M_\odot$ results in an increase in the size of the bump. In the case of the star of 1.3 $M_\odot$, there is a decrease in luminosity of 0.08 $L_\odot$, a decrease of 0.05 $L_\odot$ for a mass of 1.8 $M_\odot$ and a decrease of 0.19 $L_\odot$ in the case of the star of 2.2 $M_\odot$. In

order to know the bump behaviour for a new mass it would be necessary to run a new model, as the relation between total mass of the star and the size of the bump is not direct.

To understand these two aspects of the differences between the bumps of the different masses studied, an examination of the hydrogen abundance profile of each of these stars is required.

Figure 9 shows the abundance of hydrogen as a function of mass. Since four stars of different masses are being studied, it is more interesting to look at mass dependence and not at fractional mass as it is the case for all the other hydrogen abundance profiles presented in the other sections. The four profiles, one for each of the masses studied, are plotted on the same graph to facilitate comparison between them. To get a better view of the interesting part of the profiles, the graph shows them only up to a mass of 0.4 $M_{\odot}$. Above this mass and for the four stars, the abundance of hydrogen is constant up to the their surface. Profiles are taken when the maximum depth of the convective envelope is reached and before the hydrogen burning shell meets the chemical discontinuity in order to see the discontinuity. From left to right, we have the profile of star 1.0 $M_{\odot}$, star 1.3 $M_{\odot}$, star 1.8 $M_{\odot}$ and star 2.2 $M_{\odot}$, respectively represented by the purple, green, blue and yellow lines.

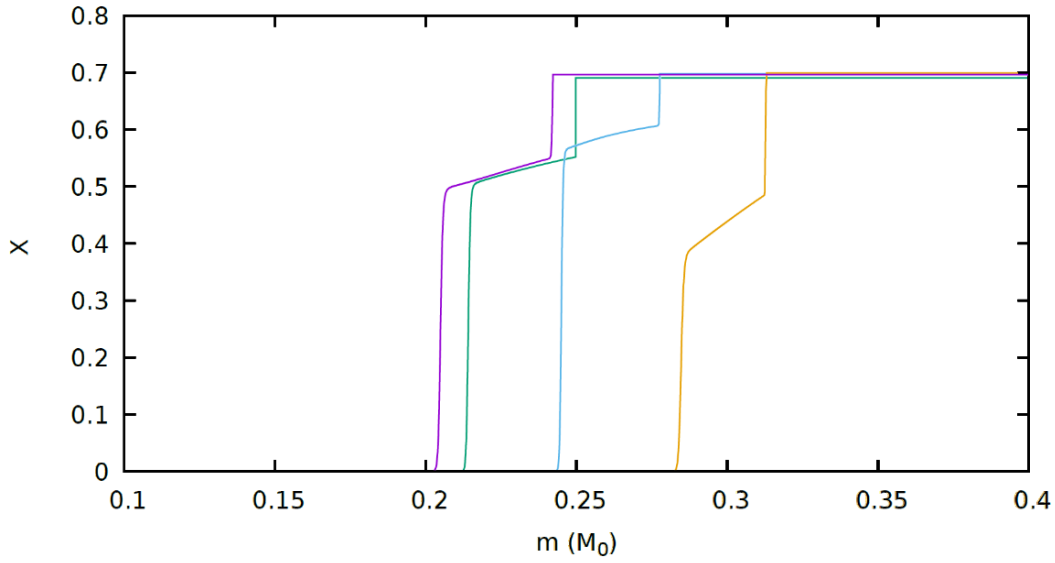

Figure 9: From the left to the right, the hydrogen abundance in function of the mass in solar mass for the 1.0 $M_\odot$, 1.3 $M_\odot$, 1.8 $M_\odot$ and 2.2 $M_\odot$ star, respectively represented by the purple, green, blue and yellow lines.

Regarding the first aspect, the fact that the luminosity of the star during the bump is higher for heavier stars, it is easily observable that the discontinuity is located at a higher mass for more massive stars. Indeed, the discontinuity is located at mass of approximately 0.24 $M_\odot$, 0.25 $M_\odot$, 0.28 $M_\odot$ and 0.32 $M_\odot$ for stars of total mass 1.0 $M_\odot$, 1.3 $M_\odot$, 1.8 $M_\odot$ and 2.2 $M_\odot$ respectively. This means that, when the H-burning shell reaches the discontinuity, the isothermal helium core is heavier for more massive stars, resulting in a higher shell temperature for these stars, according to equation (22), and the luminosity is then higher, according to equation (29).

For the second aspect, the size of the bump, it has been shown by the equations (22) and (29) that luminosity is proportional to the average molecular weight. Figure 9 shows that the discontinuity in the abundance of hydrogen does not always have the same size. A larger discontinuity, corresponding to greater increase in hydrogen, leads to a greater decrease in the average molecular weight and thus a greater decrease in luminosity, represented by a larger bump size on the HR diagram.
In Figure 9, the discontinuities of stars 1.0 $M_\odot$ and 1.3 $M_\odot$ have almost

the same size, which is also the case for their bump. For the 1.8 $M_\odot$ star, the discontinuity is much smaller than for the previous two stars, resulting in a smaller decrease in luminosity. On the contrary, for the 2.2 $M_\odot$ star, the discontinuity is much larger, resulting in a greater decrease in luminosity.

The total mass is therefore a parameter that has a great influence on the bump. As a reminder, the total mass not only influences the size of the bump and the luminosity at which it occurs, but also the appearance of the bump itself. As explained in section 3.1, a star with a mass of less than $0.08M_\odot$ does not ignite hydrogen combustion, so the bump does not occur. For too high mass, as explained in Section 4.3 and illustrated in Figure 4 for a star of $2.5M_\odot$, the bump does not occur due to the start of helium combustion in the core before the H-burning shell reaches the hydrogen abundance discontinuity.

5.2 The overshooting

As explained in section 3.2.3, overshooting can occur when there is a convective core during the main sequence and it consists in the fact that the material goes beyond the boundary of this core. The overshooting parameter α has been introduced in equation (20). To study the effect of the overshooting on the bump, the overshooting parameter was set to a value of 0.2. This value of 0.2 was chosen in order to have a sufficiently marked effect to be observed while remaining plausible. The effect was studied for a 1.3 $M_\odot$ star and a $1.8M_\odot$ star. Since overshooting is related to the convective core, for the same overshooting parameter, the observed effects are greater when the convective core is larger. Therefore, since the convective core is larger for a more massive star, the effect of overshooting is greater for the 1.8 $M_\odot$ star than for the 1.3 $M_\odot$ star. So let's start with the most interesting case, that of 1.8 $M_\odot$, and look at the case of a 1.3 $M_\odot$ star afterwards to compare the effects.

Figure 10 shows the tracks in the HR diagram for a $1.8M_\odot$ star both with and without overshooting, respectively represented in green and in purple.

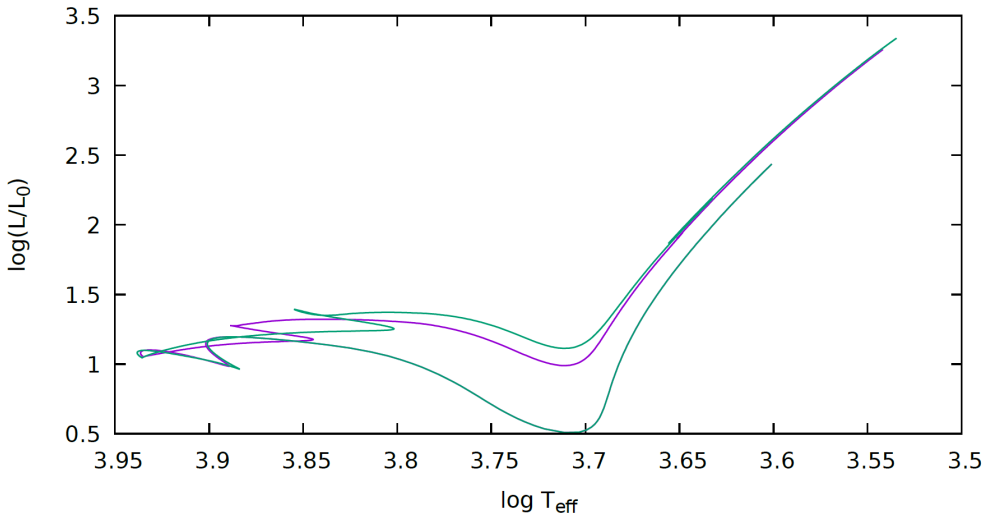

Figure 10: Tracks in the HR diagram for a $1.8M_{\odot}$ star both with and without overshooting, respectively represented in green and in purple.

Since the convective core, and thus the overshooting, only appears in the main sequence, it is natural that the two tracks overlap perfectly during the pre main sequence. Once the main sequence is reached, the two tracks differ significantly. For a $1.8M_{\odot}$, the effect is such that it is still visible at the end of the post-main sequence.

Figure 11 shows the abundance of hydrogen in function of the fractional mass at the end of the main sequence for both with and without overshooting, respectively represented in green and in purple.

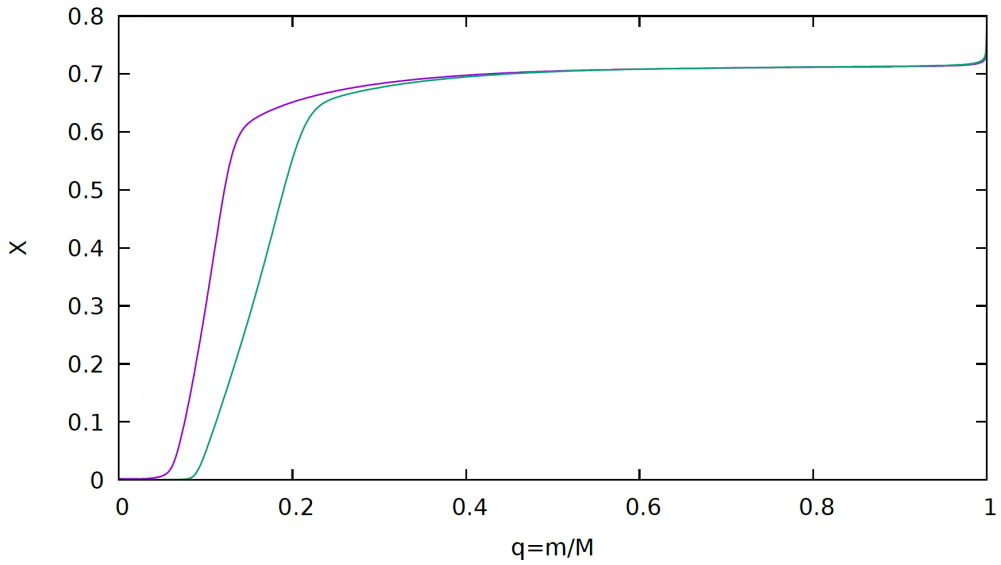

Figure 11: Abundance of hydrogen in function of the fractional mass for a $1.8M_{\odot}$ at the end of its main sequence for both with and without overshooting, respectively represented in green and in purple.

This profile shows that the presence of the overshooting is equivalent to a larger convective core. Indeed, the zero hydrogen abundance plateau goes further in the star in presence of overshooting. The post-main sequence being rather short, it is with the same type of profile that the star starts its ascent on the red giant branch. The latter is then impacted by this difference in profile, especially during the bump.

Figure 12 shows the same HR diagram as previously but zoomed in on the bump.

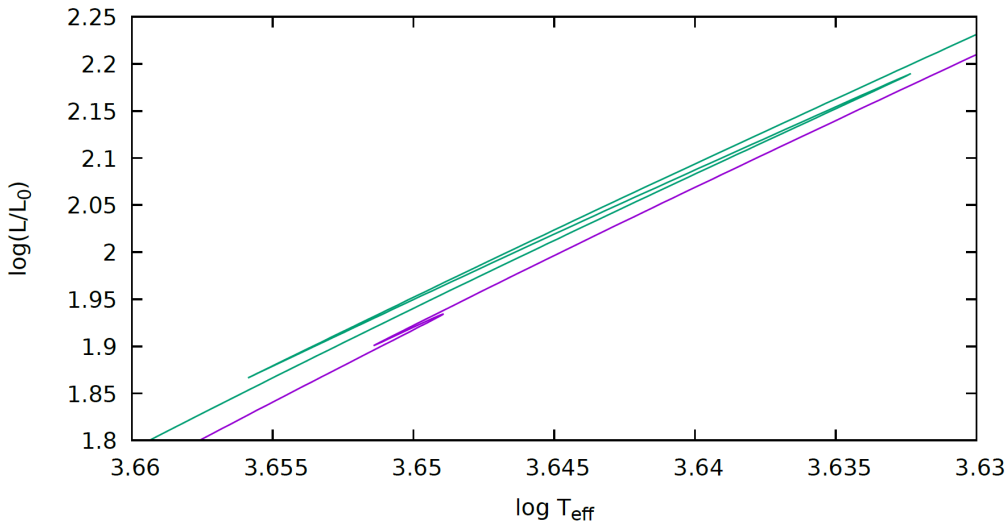

Figure 12: Tracks in the HR diagram, zoomed in on the bump, for a $1.8M_{\odot}$ star both with and without overshooting, respectively represented in green and in purple.

It can be seen that for the $1.8M_{\odot}$ star, the presence of the overshooting has a significant impact on the bump. With the overshooting, the bump starts at a much higher luminosity (almost $2.2L_{\odot}$ instead of 1.93 $L_{\odot}$) and the decrease in luminosity during the bump is much more important as well (0.32 $L_{\odot}$ in place of 0.05 $L_{\odot}$) .

Figure 13 shows the profile of the hydrogen abundance when the convective envelope have reached its maximal extension. In purple is represented the profile of the star without undershooting and in green the profile of the star with overshooting.

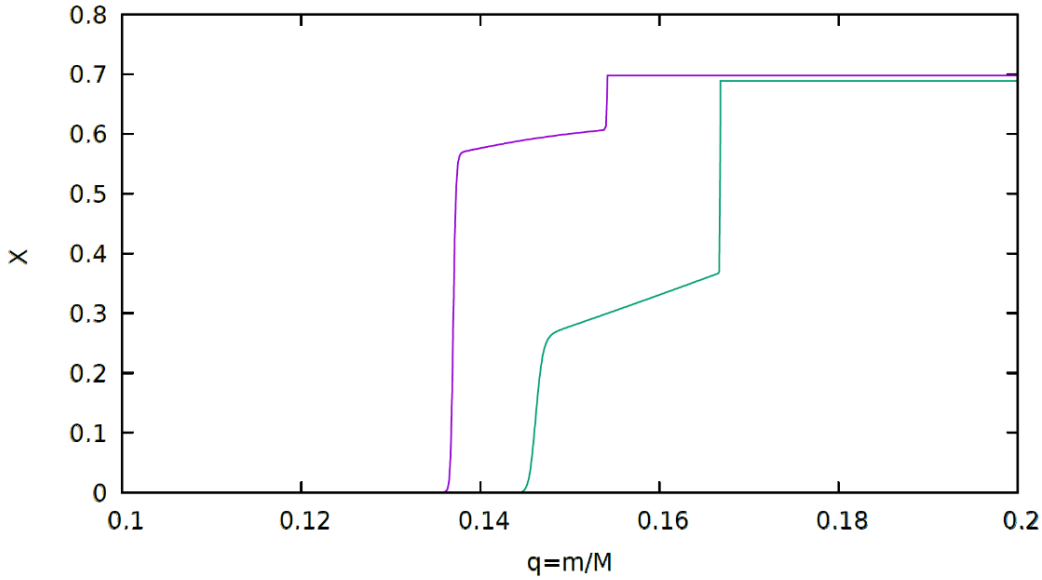

Figure 13: Hydrogen abundance in function of the fractional mass q=m/M when the convective envelope have reached its maximal extension for a $1.8M_{\odot}$ star, in purple without overshooting and in green with overshooting.

The convective envelope does not reach as deep a layer when overshooting occurs ($q \simeq 1.65$) as it does when there is no overshooting ($q \simeq 1.55$). As explained in section 4.1, as the shell progresses outward, the envelope is stopped in its descent because the temperature rises below its limit. In our case with overshooting, Figure 11 shows that, at the end of the main sequence, the convective core is larger when overshooting is present, so the temperature is higher in higher layers in the case with overshooting than in the case without. This is not only true at the end of the main sequence but also during the H-burning shell progression. The fact that there are higher temperatures in higher layers makes the envelope stop less deeply in the star. The core then has a higher mass, thus also a higher temperature (see equation (22)), when the H-burning shell reaches the discontinuity. It means that at the beginning of the bump, a star with overshooting has already reached a higher luminosity (see equation (29)) than a star without overshooting.

The importance of the discontinuity in the case of an overshooting is much greater than in the case of no overshooting. The explanation can be found in the hydrogen abundance profile at the end of the main sequence

(see Figure 11). Overshooting leads to consumption of hydrogen from the upper layers. When the convective envelope goes deeper into the star, at the layer reached by the base of the envelope, more hydrogen has been consumed in case of overshooting. The difference in hydrogen abundance before and after the envelope has reached this layer is then greater, resulting in a greater discontinuity in the profile. The increase in hydrogen abundance is then greater, so there is a greater decrease in the mean molecular weight. According to equation (22), this greater decrease in the mean molecular weight leads to a greater decrease in the temperature in the H-burning shell and thus to a greater decrease in the luminosity of the star, according to equation (29).

For comparison purposes, the case of a star of 1.3 $M_\odot$ is now being examined.

Figure 14 shows the track in the HR diagram for 1.3 $M_\odot$ stars with or without overshooting, the case with is marked in green and the case without is marked in purple.

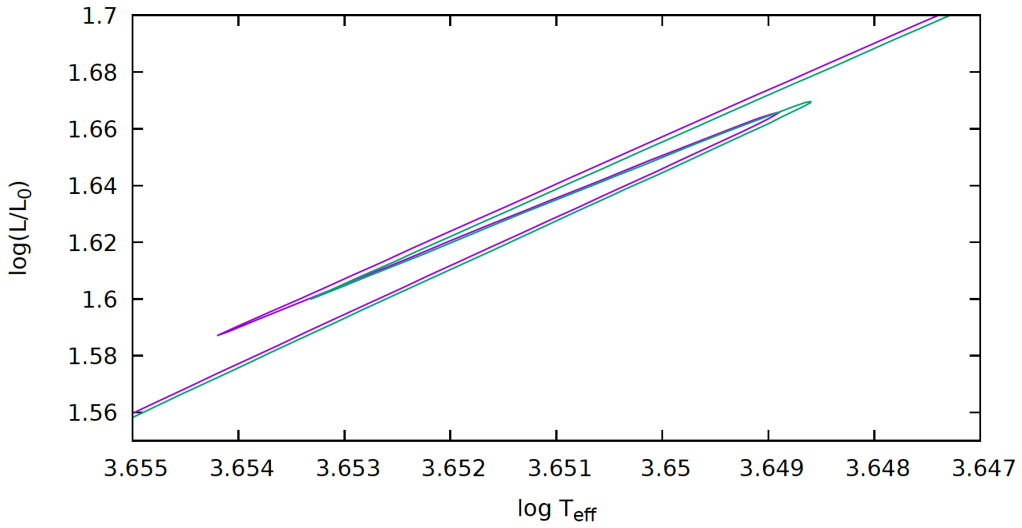

Figure 14: Tracks in the HR diagram, zoomed in on the bump, for a $1.3 M_{\odot}$ star both with and without overshooting, respectively represented in green and in purple.

As expected, the effect on the bump in the case of a 1.3 $M_{\odot}$ star is much less visible than in the case of a 1.8 $M_{\odot}$ star. As in the other case, it can be noticed that there is a higher luminosity at the beginning of the bump when overshooting is present, even if the difference is smaller. Indeed, this time the beginning of the bump occurs at a luminosity of 1.67 $L_{\odot}$, which is only 0.01 $L_{\odot}$ higher than the case without overshooting. On the other hand what is very interesting to note is that this time, instead of increasing the size of the bump, it decreases it. Only a decreasing of 0.07 $L_{\odot}$ occurs when it is worth 0.08 $L_{\odot}$ without overshooting.

Figure 15 represents the hydrogen profile as a function of the fractional mass q=m/M at the maximum descent of the envelope for a 1.3 $M_{\odot}$, with or without overshooting, respectively shown in green and purple.

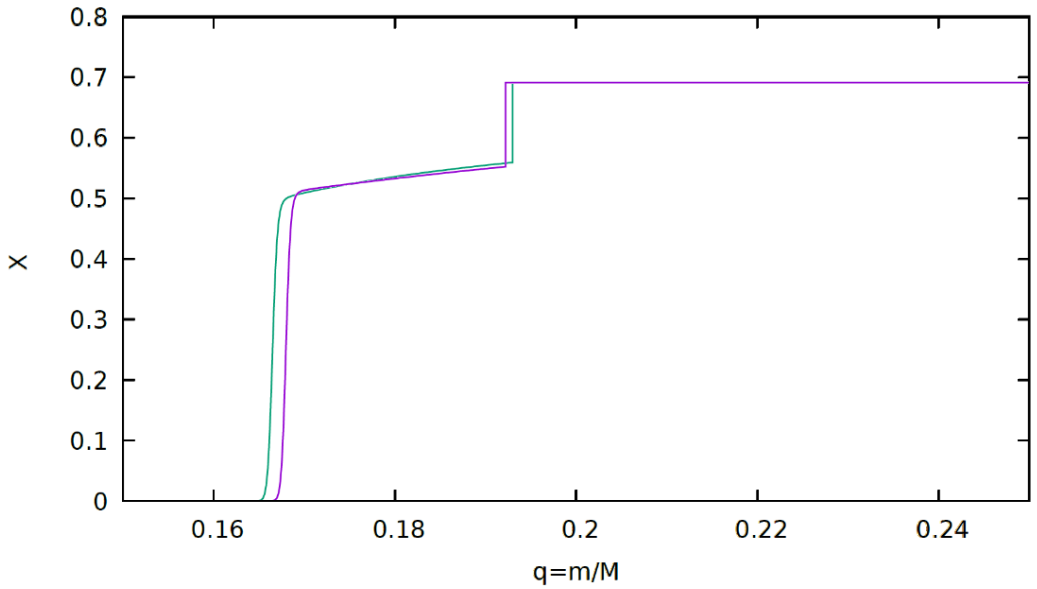

Figure 15: Hydrogen abundance in function of the fractional mass q=m/M when the convective envelope have reached its maximal extension for a $1.3 M_{\odot}$ star, in purple without overshooting and in green with overshooting.

As in the case of 1.8 $M_{\odot}$, the presence of overshooting has the same effect as if the core were larger during the main sequence. At the end of the main sequence the helium isothermal core is larger and the base of the envelope does not descend as deeply into the star. It can be seen that this is the case in figure 15, even though the difference in depth is much less than for the 1.8 $M_{\odot}$ star. What differs however is that the discontinuity is smaller here than in the previous case. The case with overshooting indeed consumes hydrogen in upper layers compared to the case without overshooting. Nevertheless, the impacted zone does not extend to the layers affected by the convective envelope. The difference between the amount of hydrogen before and after the envelope reaches its maximum depth is therefore less, leading to a smaller discontinuity. In the case of the 1.3 $M_{\odot}$ star, the discontinuity is slightly smaller when overshooting is present than when there is none. This explains why overshooting leads to a slightly smaller decrease in luminosity during the bump, using the same reasoning than for a 1.8 $M_{\odot}$ star, but this time with a mean molecular weight which decreases less than without overshooting.

The difference brought by overshooting is therefore not only more or less important from one mass to another but also different, leading in one case to an increase in the size of the bump and in the other to its decrease.

As discussed in section 4.3, for high-mass stars, the helium core reaches such a size that the temperature is high enough for helium burning to begin before the H-burning shell has reached the discontinuity, resulting in the absence of a bump. In addition, it was also noted above that the presence of overshooting causes the core to become larger, and therefore hotter, when the H-burning shell reaches the discontinuity. A third case is therefore worthy of consideration: the 2.2 $M_{\odot}$ star with overshooting.
As mentioned in section 5.1, a 2.2 $M_{\odot}$ star has a mass that is still low enough for the bump to occur. Nevertheless, this mass is close to the limit above which no bump is visible. A model for a 2.2 $M_{\odot}$ star with an overshooting parameter $\alpha = 0.2$ has been run. For this model, the overshooting causes the core to become massive enough, and therefore hot enough, to trigger helium combustion before the discontinuity has been reached by the H-burning shell. In this model, no bump occurs.

Figure 16 shows the hydrogen abundance profile as a function of the fractional mass q=m/M for the model of a 2.2 $M_{\odot}$ star with an overshooting parameter $\alpha = 0.2$ when the helium burning is onset.

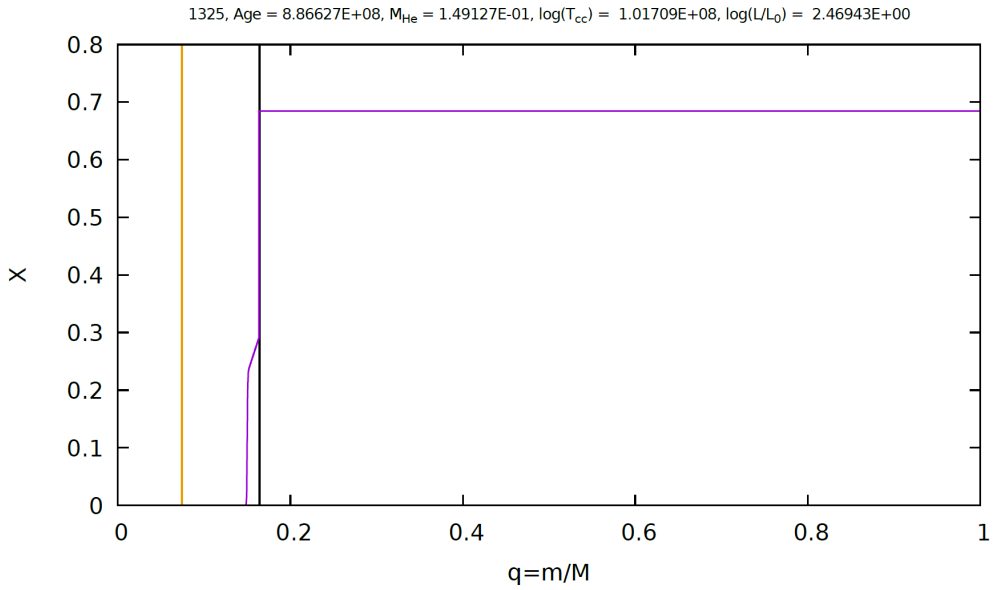

Figure 16: Hydrogen abundance in function of the fractional mass q=m/M for a 2.2 $M_{\odot}$ once the helium burning is onset. The yellow vertical line represents the limit of the convective core.

The yellow line represents the convective core. If convection occurs, it means that the core cannot be isothermal, so helium burning is present in the core. The helium burning shell and the discontinuity are both easily identifiable, it can be seen that the first one has not yet met the second one, the bump may not have occurred.

5.3 The undershooting

As described in section 3.2.3, the undershooting is a phenomenon that can occur when there is a convective envelope. The structure of a star during the red giant phase has also been described in section 4.1 and it has been shown that the outermost layer is a convective envelope. As a reminder, in a convective region, energy is transported by the motion of matter. Undershooting occurs when matter still moves beyond the lower boundary of the convective envelope.
The undershooting parameter α has also been defined. For this study of the

influence of undershooting on the bump, two different values were chosen for the undershooting parameter: $\alpha = 0.2$ and $\alpha = 0.4$. As with overshooting, these values were chosen to ensure that the effect is sufficiently observable yet plausible.

In our models, undershooting is only activated once the red giant branch is reached. The three tracks are then overlaid in the HR diagram for different values of the undershooting parameters until they reach the branch of the red giant. The HR diagram can therefore be examined directly at the red giant branch where an effect due to undershooting is clearly visible on the bump.

Figure 17 shows the tracks in the HR diagram around the bump for a 1.3 $M_\odot$ star with an undershooting parameter $\alpha = 0.2$ in green, $\alpha = 0.4$ in blue and without undershooting in purple.

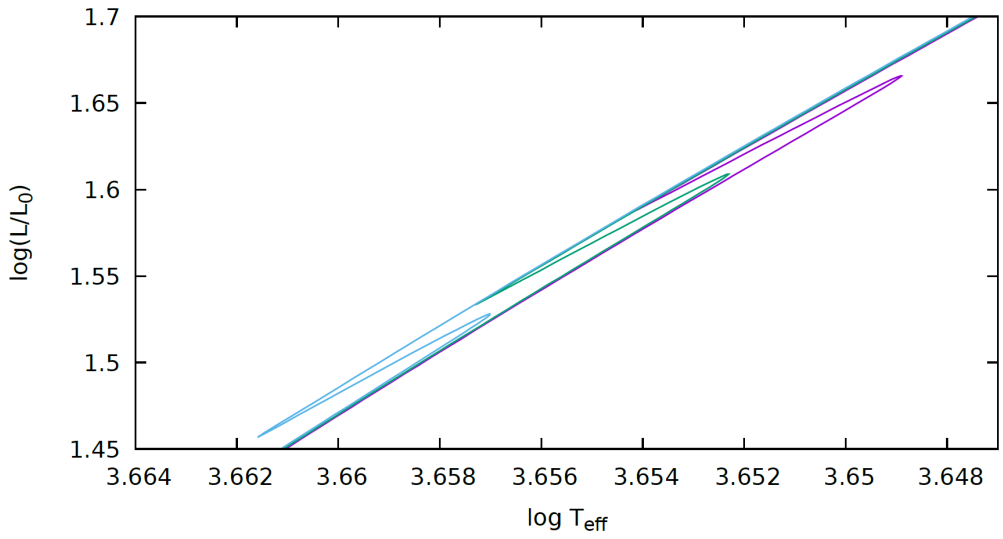

Figure 17: Zoom on the part of the red giant branch of the tracks in the HR diagram for a 1.3 $M_\odot$ star with an undershooting parameter $\alpha = 0.2$ in green, $\alpha = 0.4$ in blue and without undershooting in purple.

It has been seen in section 4.2 that the key element in the red giant bump

is the presence of a discontinuity in hydrogen abundance. This discontinuity is left by the deepening of the convective envelope down to a maximum depth fixed by the outwards motion of the H-burning shell. The location of the discontinuity is thus the lower boundary of the convective envelope at its maximum extension. As the undershooting extends the full mixing region, the higher the undershooting parameter, the deeper is the discontinuity, as can be seen in the following figure.

Figure 18 shows the hydrogen abundance in function of the fractional mass for the case without undershooting in purple and for an undershooting parameter $\alpha = 0.2$ and $\alpha = 0.4$ in green and blue respectively. It can be seen that the discontinuity, initially just above q=0.19, drops a little bit below q=0.19 for $\alpha = 0.2$ and up to q=0.185 for $\alpha = 0.4$.

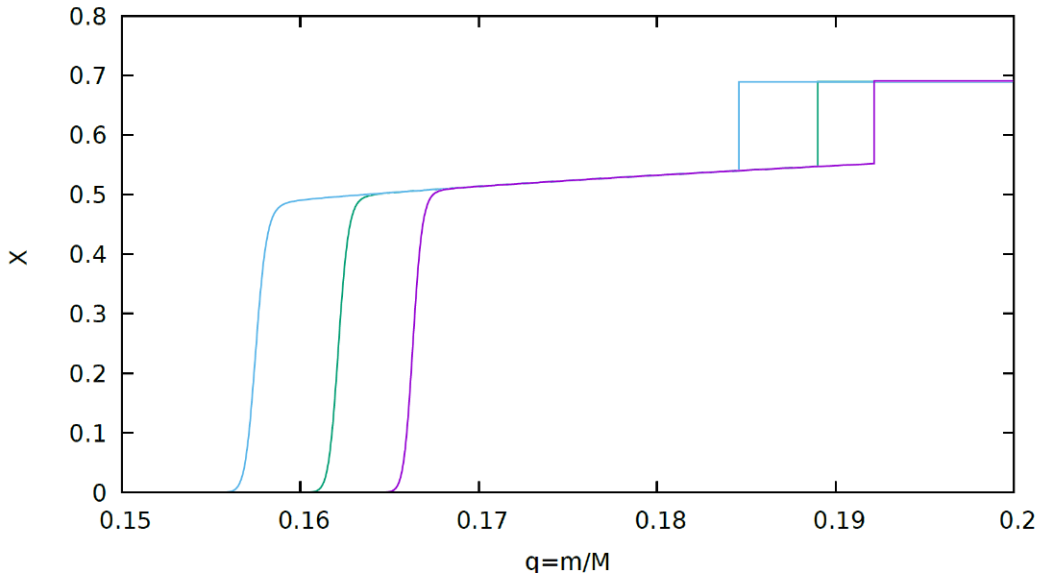

Figure 18: Hydrogen abundance in function of the fractional mass q=m/M for a 1.3 $M_\odot$ star. The purple profile represents the case without undershooting, the green and blue profiles represent respectively the case with an undershooting parameter $\alpha = 0.2$ and $\alpha = 0.4$

With the discontinuity being closer to the center, it is natural that the H-shell, going outward, encounters the discontinuity sooner. It has been seen in the description of the red giant branch (see section 4.1) that, except for

the moment during which the star undergoes the bump, the luminosity of the star increase. An earlier encounter between the H-shell and the discontinuity then obviously occurs at a lower luminosity. This can be explained with equations (22) and (29). At the time of the encounter, this one occurring earlier, the core is smaller, the temperature is therefore lower in the shell and thus the luminosity is also lower. The figure 15 shows indeed that for higher undershooting parameter, the luminosity at which the bump begins is lower.

The situation can also be seen from another point of view. Let's take a fixed luminosity, for instance $L = 1.56 L_{\odot}$.

Figure 19 shows the profiles of hydrogen abundance as a function of the fractional mass q=m/M in a 1.3 $M_{\odot}$ star with a luminosity $L = 1.56 L_{\odot}$. The case without undershooting is shown in purple, with an undershooting parameter $\alpha = 0.2$ in green and with an undershooting parameter $\alpha = 0.4$ in blue. There are three hydrogen abundance profiles when the undershooting parameter is $\alpha = 0.2$. This is explained by the fact that a star with such an undershooting parameter will pass three times through the fixed luminosity value L=1.56 while stars without overshooting or with an undershooting parameter $\alpha = 0.4$ will pass only once through this luminosity. The numbers next to the green profiles indicate the moment that the profile represents. Profile number 1 is obtained before the bump, profile number 2 is obtained during the bump and finally profile number 3 is obtained after the bump.

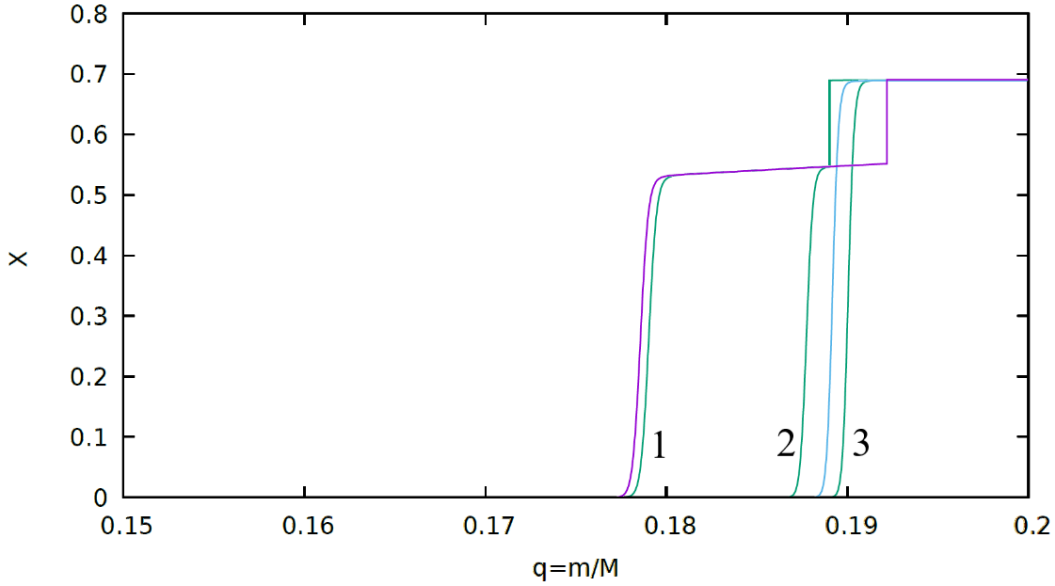

Figure 19: Profiles of hydrogen abundance as a function of the fractional mass q=m/M in a 1.3 $M_\odot$ star with a luminosity $L = 1.56 L_\odot$, without undershooting in purple, with an undershooting parameter $\alpha = 0.2$ in green and with an undershooting parameter $\alpha = 0.4$ in blue. The numbers next to the green profiles indicate the moment that the profile represents. Profile number 1 is obtained before the bump, profile number 2 is obtained during the bump and finally profile number 3 is obtained after the bump.

Let's imagine a star at the bottom of the branch of the red giants, so with a low luminosity. The H-burning shell progresses outwards while the star progresses on the RGB and the luminosity thus increases.

In the case of an undershooting parameter $\alpha = 0.4$, we find ourselves in the case where the envelope has descended the deepest into the star and in this case. Once a luminosity of about L=1.53 $L_\odot$ is reached, the shell meets the hydrogen abundance discontinuity. So the bump occurs and the luminosity decreases then increases afresh. The H-burning shell continues to progress and once the luminosity of 1.56 $L_\odot$ is reached, the hydrogen abundance profile is as shown in blue in figure 17.

Let's take the same reasoning but with an undershooting parameter of $\alpha = 0.2$. Starting from the bottom of the RGB, the shell progresses, the luminosity increases until the luminosity of L=1.56 $L_\odot$ is reached. Contrary to

the previous case, the discontinuity has not yet been reached. The hydrogen abundance profile is then as shown in green in figure 17 with the number 1. The luminosity continues to increase and we reach a luminosity of about L=1.61. The H-burning shell then meets the discontinuity and the luminosity decreases. As it decreases, it reaches again a luminosity of L=1.56 $L_{\odot}$. The hydrogen abundance profile is then at that moment as represented by the green profile next to number 2. Once the luminosity of about L=1.54 $L_{\odot}$ is reached, it will increase again and thus pass again through a luminosity of L=1.56 $L_{\odot}$, this time with a profile such as the green one next to number 3.

Let's use the same reasoning again but this time with the case where there is no undershooting. In this case, the H-burning shell progresses and the luminosity increases, until a luminosity of L=1.56 $L_{\odot}$ is reached. Since the shell has not yet reached the discontinuity, the bump does not take place yet. The hydrogen profile at this point is such that the purple profile in figure 17. The discontinuity is even further away than in the previous case and it is necessary to wait for a luminosity of about L=1.66 $L_{\odot}$ for the bump to start. We then have a decrease in luminosity but not enough to have a luminosity of L=1.56 $L_{\odot}$ again.

This explains why we have three times the luminosity of L=1.56 $L_{\odot}$ for an undershooting of $\alpha = 0.2$ and only once in the other two. It can also be seen in the HR diagram (see figure 15) that if we draw a horizontal line with a value of L=1.56 $L_{\odot}$, the purple and blue tracks would cross the line only once, while the green track would cross it three times.

Although changing the luminosity at which the bump occurs, it can be seen in figure 16 that the size of the discontinuity remains the same in the three cases presented and the decrease in luminosity will therefore be the same whether or not there is undershooting and regardless of its undershooting parameter.

5.4 The metallicity

The metallicity represent the proportion of all the elements heavier than hydrogen and helium. At the beginning of the Universe, as a result of primordial nucleosynthesis, matter was composed almost exclusively of hydrogen and helium with only a very small amount of lithium, beryllium and boron. The metallicity of the first stars was then very close to zero. It is in the stars that

heavier elements are formed through nuclear reactions and neutron capture essentially. These elements may later be found in the interstellar medium, after having been ejected from stars via, for example, supernovae at the end of the life of massive stars. From this interstellar medium, new stars may be formed, with a higher metallicity. We have thus stars forming at different times and different places, which affect its metallicity. The metallicity stays nevertheless quite small, the hydrogen and the helium staying the two main components of stars at their formation, but it is enough to see differences between stars with different metallicity. An example of composition to see this dominance of hydrogen and helium is the composition of the surface of the Sun which is: $X_{Sun} = 0.7381$, $Y_{Sun} = 0.2485$ and $Z_{Sun} = 0.0134$ (Asplund et al., 2009).

As already seen, mean molecular weight is an important parameter in the study of the bump. Changing metallicity theoretically changes the mean molecular weight, but metallicity being so small compared to the abundance of hydrogen (and helium) that this change will not be seen. However, one factor that changes much more with metallicity is opacity as described by the Kramer's law (see equation (17)).

In this study, three different metallicities have been chosen: Z=0.015, Z=0.01 and Z=0.005. The first one, Z=0.015, is our basic metallicity: except in this part in which the metallicity is studied, it is the one used to model all the other stars.

Figure 20 shows the tracks of three stars of 1.8 $M_{\odot}$ having as only difference their metallicity. The purple track represent the star with a metallicity Z=0.015, the green one is for Z=0.01 and finally the blue one is for Z=0.005.

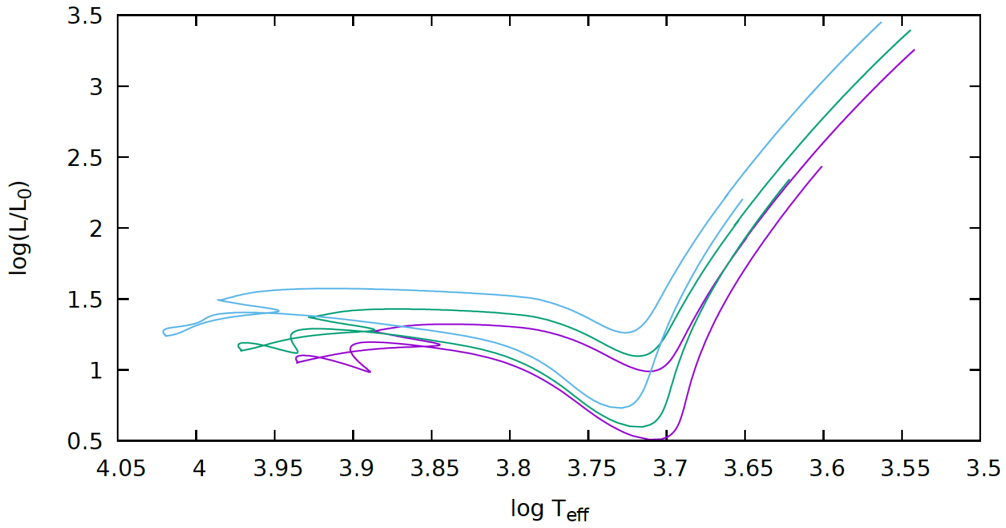

Figure 20: Tracks in the HR diagram of a 1.8 $M_{\odot}$ star with a metallicity Z=0.015 (purple), Z=0.01 (green) and Z=0.005 (blue).

As for the study of the total mass influence, the change of metallicity affects the star on its global evolution. The tracks undergoes a translation towards higher luminosities and temperatures when the chosen metallicity is lower. Even if it is less significant than in the study of the total mass, a difference in the shape of the tracks during the main sequence is also observable.

Figure 21 shows the same tracks but zoomed in on the part where the bump is happening.

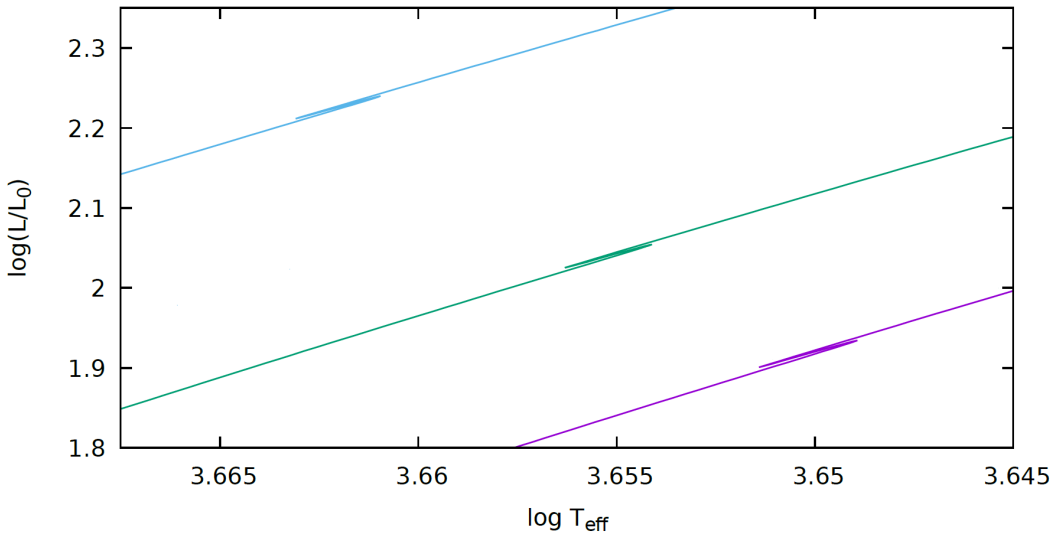

Figure 21: Tracks in the HR diagram, zoomed in on the bump, of a 1.8 $M_{\odot}$ star with a metallicity Z=0.015 (purple), Z=0.01 (green) and Z=0.005 (blue).

As with the rest of the evolution of these stars, it is observed that the bump occurs at lower luminosity if the metallicity is higher. For a metallicity Z=0.005 the bump begins at a luminosity L=2.24 $L_{\odot}$, for Z=0.01 at L=2.05 $L_{\odot}$ and for Z=0.015 at L=1.93 $L_{\odot}$. Regarding the decrease in luminosity, all three cases show the same decrease.

Figure 22 shows the hydrogen abundance in function of the fractional mass q=m/M. Each of them is taken when the convective envelope is at its maximum extend. The same correspondence is used between the color of the profile and the metallicity as for the HR diagrams.

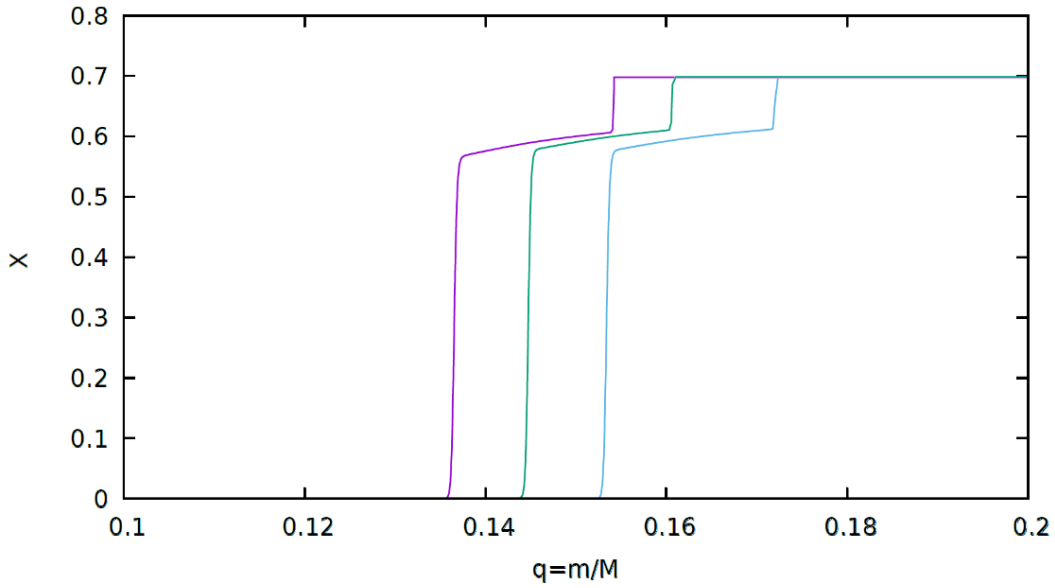

Figure 22: Hydrogen abundance in function of the fractional mass q=m/M at the maximum extend of the convective envelope for a 1.8 $M_{\odot}$ star with a metallicity Z=0.015 (purple), Z=0.01 (green) and Z=0.005 (blue).

These three profiles show that the convective envelope is deeper in a higher metallicity star than in a lower metallicity star. The discontinuity is near q=0.17 for Z=0.005, near q=0.16 for Z=0.01 and near q=0.155 for Z=0.015. This behaviour comes from the dependence between metallicity and opacity, as described by Kramers' law (see equation (17)). Due to their high ionization potential, heavy elements increase opacity. Opacity is involved in the expression of the radiative temperature gradient (equation (6)), the latter being directly proportional to opacity. A higher metallicity then leads to a higher radiative temperature gradient. According to the Schwarzshild criterion (equation (5)) the convective zone, in this case the convective envelope, is more extensive and the discontinuity is lower in the star. As seen in the case of undershooting, a lower discontinuity leads to a lower luminosity at the beginning of the bump because the discontinuity is reached earlier. So, a higher metallicity leads to a lower luminosity of the star at the beginning of its bump.

Another explanation which may be complementary to the previous reasoning, is that for higher metallicity the core has a smaller mass when the

bump happens. Indeed, for the metallicities Z=0.015, Z=0.01 and Z=0.005, the isothermal helium core at the moment of the bump has respectively a mass of $M_{He} = 0.149M_{\odot}$, $M_{He} = 0.159M_{\odot}$ and $M_{He} = 0.169M_{\odot}$. As the luminosity is link to the mass of the core via equations (22) and (29), it corresponds well to what is observed. For a higher Z, the opacity is greater (see equation (6)), and the luminosity being inversely proportional to the opacity, the luminosity is lower. Less nuclear power is then required to provide the luminosity. This leads to the fact that the CNO cycle is less active, which implies a lower temperature in the core layers. The convective core is then less massive during the main sequence. Therefore, at the end of the main sequence, the helium core is also less massive. According to equations (22) and (29), the shell temperature is lower and therefore the luminosity of the star is also lower.

The hydrogen profile also shows that the size of the discontinuity is the same for our three metallicities. This is consistent with the fact that we see the same decrease in luminosity during the bump for all three cases.

5.5 Diffusion

5.5.1 Microscopic diffusion

Diffusion is described in section 3.2.4. As a reminder, it is a phenomenon that brings light elements upwards and heavy elements downwards. Microscopic diffusion thus has an impact on the hydrogen abundance profile, but since diffusion is slow in the deep layers of the star, its impact is quite small.

To see the impact of microscopic diffusion, two evolutionary models for a $1.3M_{\odot}$ star are compared, one with microscopic diffusion, the other without. To be noted that microscopic diffusion is always present in stars, so it is taken into account in all the other models presented in this study.

Figure 23 represents the tracks in the HR diagram of a 1.3 $M_{\odot}$ star with and without microscopic diffusion, in purple and green respectively.

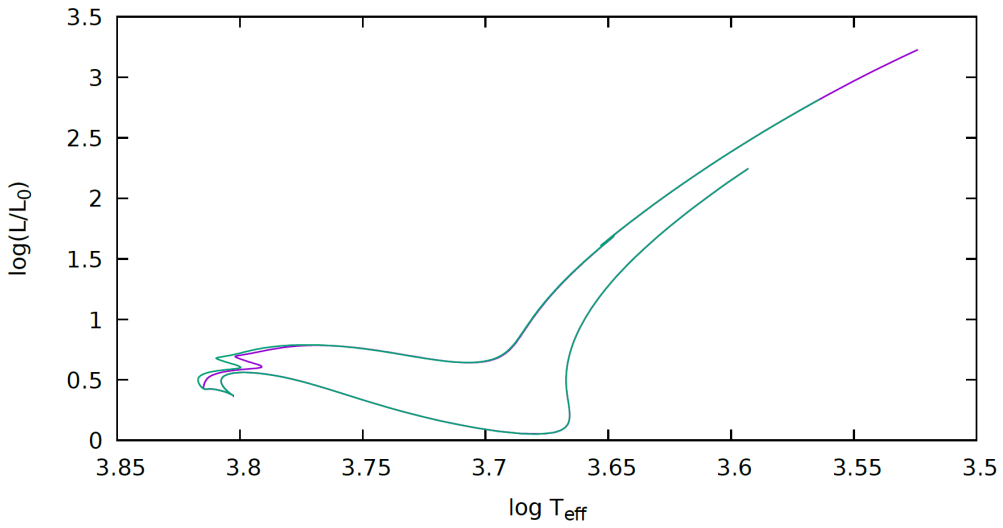

Figure 23: Tracks in the HR diagram of a 1.3 $M_\odot$ star with and without microscopic diffusion, in purple and green respectively

It can be observed that microscopic diffusion causes a change in the evolution during the main sequence. Nevertheless, the difference between the two tracks seems to disappear during the post-main sequence. This difference during the main sequence will thus have no impact on the bump.

Figure 24 shows a zoom in on the tracks in the HR diagram around the bump.

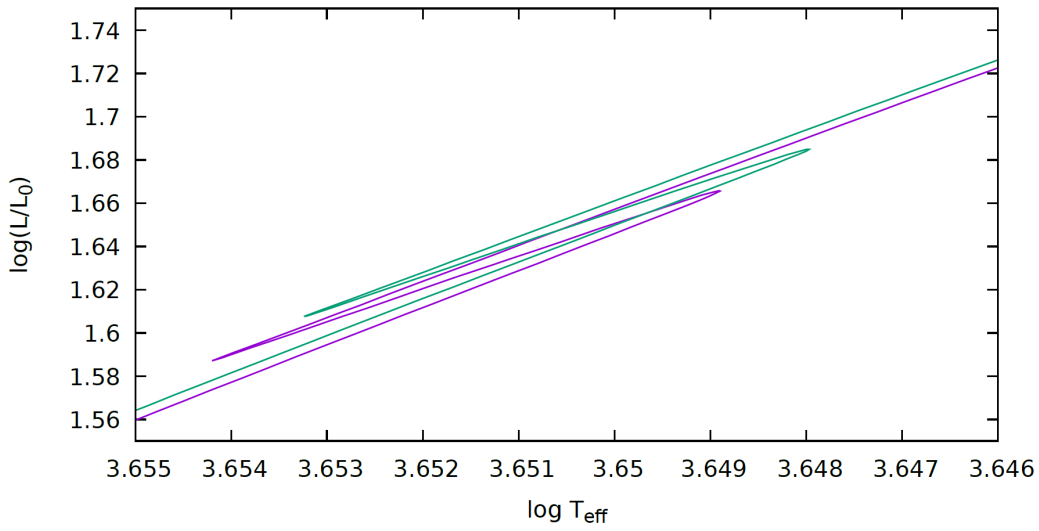

Figure 24: Tracks in the HR diagram zoomed in around the bump for a 1.3 $M_\odot$ star with and without microscopic diffusion, in purple and green respectively

The microscopic diffusion still has an impact on the bump as can be seen by looking closely, but as expected the impact is quite small. The bump starts at L=1.66 $L_\odot$ when there is microscopic diffusion and at L=1.68 $L_\odot$ when it is not taken into account. In the case of microscopic diffusion, the bump thus occurs at a slightly lower luminosity but the extent of the decrease in luminosity remains the same.

Figure 25 shows the hydrogen abundance profile in function of the fractional mass q=m/M for both with and without microscopic diffusion. Just as the HR diagram must be looked at closely enough to see a difference between the two bumps, the two profiles must also be looked at closely enough to see a difference between them.

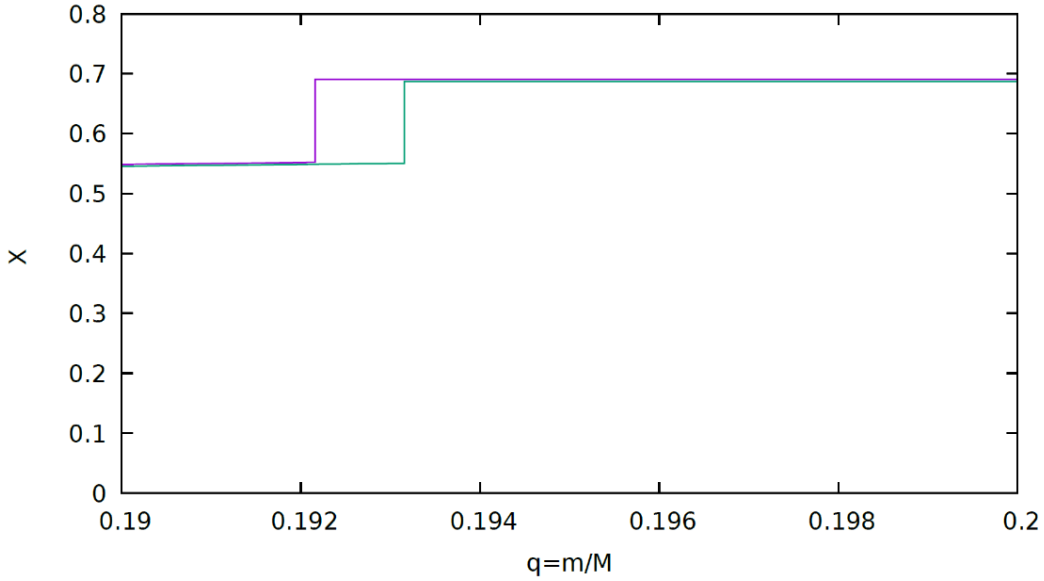

Figure 25: Hydrogen abundance in function of the fractional mass q=m/M at the maximum extent of the convective envelope for a 1.3 $M_{\odot}$ with and without microscopic diffusion, respectively in purple and in green.

As can be seen in the profiles above, the discontinuity is slightly deeper in the star (q a little bit above 0.192 $M_{\odot}$) when the microscopic diffusion is taken into account than when it is neglected (q a little bit above 0.193 $M_{\odot}$). As explained for the case of undershooting, a lower envelope leads to a sooner encounter between the H-burning shell and the discontinuity, the isothermal core is then less hot, the temperature of the shell is lower and we have a lower luminosity when the bump starts.

It can also be seen that the size of the discontinuity is the same in both cases, which is consistent with the fact that the decrease in luminosity in both cases is the same.

5.5.2 Turbulent diffusion

Microscopic diffusion is not the only type of diffusion that occurs in stars. Turbulent diffusion can occur due to shear caused by differential rotation in the star. To study specifically the effect of turbulent diffusion on the bump,

this diffusion is only introduced from the base of the red giant branch. Turbulent diffusion could be present earlier in the evolution of the star, but taking it into account already during the main sequence, its effect would be similar to overshooting, what we want to avoid to specifically see the impact of turbulent diffusion during RGB and the bump. The star is then compared to another star in which only microscopic diffusion is present.

Figure 26 shows the tracks of the 1.3 $M_\odot$ star, with and without turbulent diffusion during the red giant branch phase.

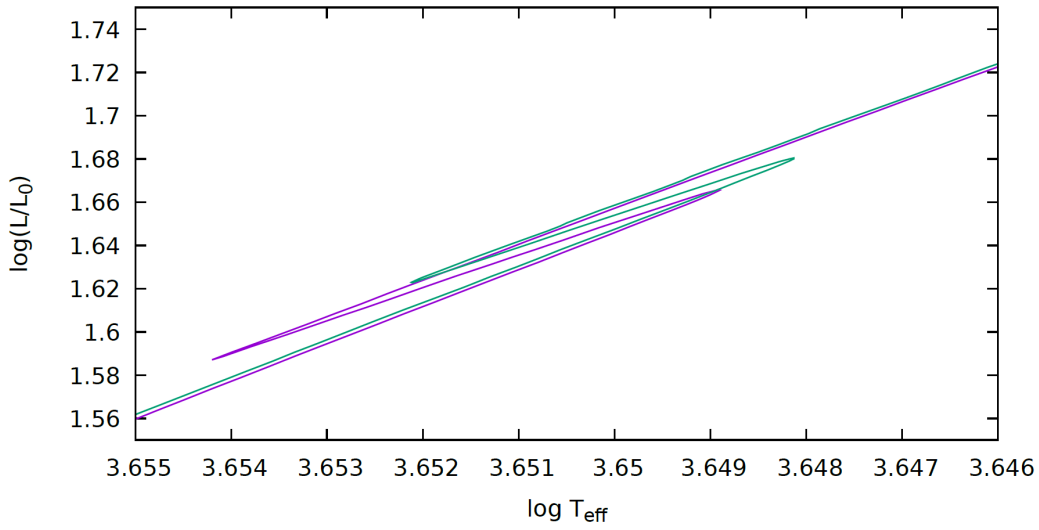

Figure 26: tracks of the 1.3 $M_\odot$ star, with and without turbulent diffusion during the red giant branch phase, in green and in purple respectively.

The difference between the two bumps is more visible than in the case of microscopic diffusion but remains less important than some other parameters studied previously. The bump starts at a higher luminosity, L=1.68 $L_\odot$, in the presence of turbulent diffusion than when there is none, L=1.66 $L_\odot$. The decrease in luminosity is less in the case of turbulent diffusion where there is a decrease of 0.06 $L_\odot$ instead of 0.08 $L_\odot$ when there is no turbulent diffusion.

Figure 27 shows the hydrogen abundance profile in function of the fractional mass q=m/M at the maximum extend of the convective envelope for the 1.3 $M_\odot$ star with and without turbulent diffusion.

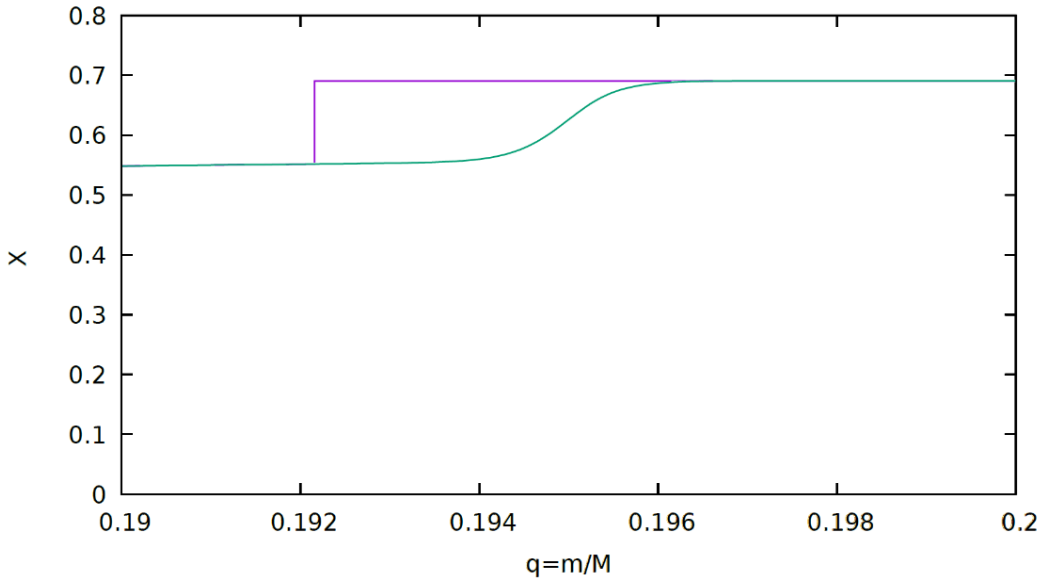

Figure 27: Hydrogen abundance in function of the fractional mass q=m/M at the maximum extend of the convective envelope for a 1.3 $M_\odot$ star with and without turbulent diffusion, respectively in green and in purple.

Two major differences can be observed in the profiles presented above. The first is that, when there is turbulent diffusion, the envelope doesn't go as deep into the star (q between 0.194 $M_\odot$ and 0.196 $M_\odot$) as when only microscopic diffusion is present (q $\simeq 0.192 M_\odot$). This then explains why the bump occurs at higher luminosity when there is turbulent diffusion. Indeed, when there is turbulent diffusion, the encounter between the H-burning shell and the chemical discontinuity happens latter in the evolution of the star, the isothermal core is then hotter, the temperature of the shell is then higher (see equation (22)) and the luminosity at the beginning of the bump is therefore higher (see equation (29)).

The second difference is the shape of the discontinuity (if it still can be called a discontinuity). While for microscopic diffusion there is a very clear discontinuity, with turbulent diffusion this discontinuity is somehow tilted leading to a smoother change in hydrogen abundance. So the mean molecu-

lar weight also changes more smoothly. It has been explained in section 4.2 that the bump occurs because of a sudden decrease in the mean molecular weight and could not be compensated quickly enough by the term $\frac{M_{core}}{R_{core}}$ in equation (22). Since μ changes more smoothly when there is turbulent diffusion, the term $\frac{M_{core}}{R_{core}}$ therefore has more time to increase as μ decreases. The decrease of μ, which is the factor leading to the decrease in temperature, and therefore in luminosity (see equation (29)), is then partially compensated. The decrease does occur but is not as strong as in the case of a steeper discontinuity.

5.6 Impact on the observations

Through the study of the impact of the various parameters, two different effects can be distinguished. The first one is a change in the luminosity at which the bump happens, the second one is a change of the size of the bump which means how important is the decrease of the luminosity before resuming to its normal increase.

The impact on the observation of the first effect is quite straightforward. Depending on the parameters of the stars composing a cluster that would be observed, the bump would occur at one luminosity or another. If a bump is detected and the value of some parameters is obtained, the luminosity of the bump can give some constraints on the unknown parameters.

For the size of the bump, the bigger it is, the wider is the range of luminosities in the bump. Then, the bigger is the bump, the more complicate it is to detect it. Indeed, it would be more difficult to detect a bump if all the stars composing it are distributed on a wide range of luminosity than if they are all at a specific or small range of luminosity. Nevertheless, if the range of luminosity for the bump can be determined during an observation, it could put some constraints on the parameters.

It should be noted that this interpretation of the impact of the change in the size of the bump on the observations assumes that the bump occurs on the same time scale. For example, when we look at the effect of overshooting for a 1.8 $M_{\odot}$ star, the duration of the bump is approximately the same whether or not there is overshooting, and the effect on the observation explained

above is valid. If we look on the other hand at the effect of mass change on the bump, the bump lasts longer for a $2.2M_{\odot}$ star than for a 1.0 $M_{\odot}$ star. The fact that the bump covers a wider range of luminosity for a 2.2 $M_{\odot}$ star would therefore perhaps be compensated by a longer time spent in this range of luminosity. However, one should also take into account the global time of stellar evolution, which is not the same for the two stars. The duration of the bump should then be compared to the stellar evolution time. We see by this example that in certain cases the impact on the observations is more complex to interpret.

6 Comparison with the literature

The starting point of this study was the reading of three articles concerning the red giant branch bump. The first one is *"The shape of the Red Giant Branch Bump as a diagnostic of partial mixing processes in low-mass stars"* by Cassisi et al. from 2001, the second one *"The magnitude difference between the main sequence turn off and the red giant branch bump in Galactic globular clusters"* by Cassisi et al. from 2011 and the last one *"The Red-Giant Branch Bump Revisited: Constraints on Envelope Overshooting in a Wide Range of Masses and Metallicities"* by Kahn et al. from 2018. Now that results has been obtained and interpreted, it is of interest to compare our results to those of these articles.

6.1 "The shape of the Red Giant Branch Bump as a diagnostic of partial mixing processes in low-mass stars" (Cassisi et al., 2001)

The purpose of the first article is to study the impact of the partial mixing processes on the red giant bump. Partial mixing includes undershooting, overshooting and diffusion. In particular here what is sought to be understood is the impact of the possible smoothing of the discontinuity left by diffusion and undershooting.

For this they will use several models whose basic model is a model for which Y=0.23, Z =0.006 and the mass of the star is 1 $M_{\odot}$. Several tests are performed by adding or not diffusion and using undershooting parameters $\alpha = 0.1$ or $\alpha = 0.2$. Whether there is diffusion or not and whether there is undershooting or not, the discontinuity remained sharp and the bump observed via the luminosity function did not change in shape, they nevertheless observed a change of the luminosity at which the bump happens. They concluded that the change in the shape of the bump was probably due to the change in sharpness of the discontinuity. In order to be able to study this characteristic, they studied new models in which undershooting and diffusion were neglected but where the hydrogen abundance just below the maximum extension of the convective envelope is artificially changed. The smoothing lengths used are 0.1 H_p , 0.2 H_p, 0.5 H_p and 0.75 H_p, where H_p is the local

pressure scale height. To simplify the study they used a linear smoothed zone and the hydrogen abundance in the envelope was modified so as not to change the total abundances of the star.

Figure 28 shows the type of hydrogen abundance profile they obtained with a smoothing parameter 0.5 H_p.

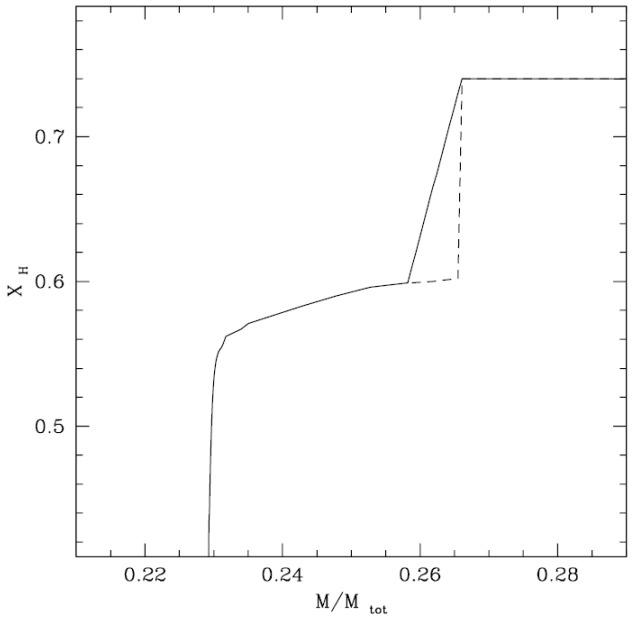

Figure 28: Hydrogen abundance in function of the fractional mass in the model used by Cassisi et al. in the presented paper. The dashed line is the model without smoothing, the solid line is for a smoothing parameter 0.5 H_p. (Cassisi et al. 2001)

From these profiles, they used a Monte Carlos technique to obtain luminosity functions.

Figure 29 shows the luminosity functions for each of the smoothing parameters used in solid line and the model without smoothing in dotted line. For artificial smoothing of the discontinuity, they also observed a change in

luminosity but shifted their results to match the brightest side to make it easier to compare the shape of the bump, which was the main goal.

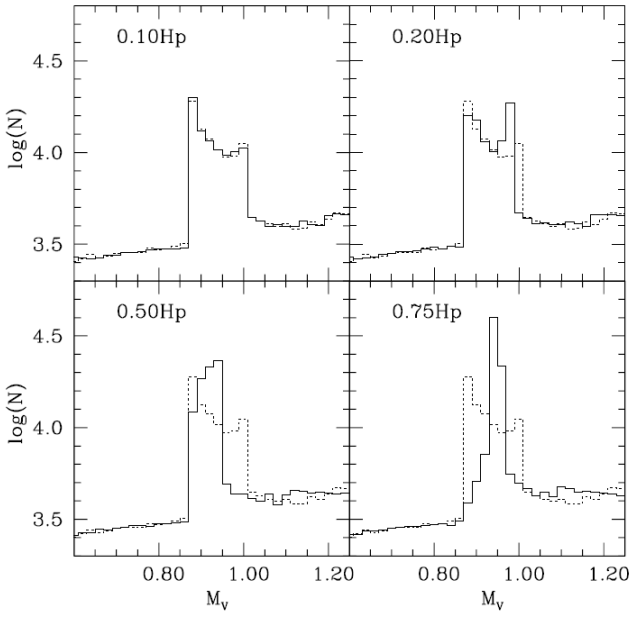

Figure 29: Comparison between the different luminosity functions simulated by the Monte Carlo technique for different hydrogen abundance profile artificially construct. (Cassisi et al. 2001)

The effect is easily visible, especially for smoothing parameters of 0.5 H_p or more. For greater smoothing, the bump is more centered and symmetrical. They conclude that the efficiency of hydrogen burning during the bump depends on the thickness of the discontinuity. The thicker the area of change in hydrogen abundance, the smaller is the efficiency variation.

They also artificially changed the opacity at the discontinuity but saw no impact on the bump. They concluded that the most important factor was therefore the change in hydrogen abundance.

Finally, they also looked at whether these differences would be visible in observations and concluded that the response depended on various parameters, including metallicity. For a globular cluster of high metallicity, the effect of a smoothing parameter of 0.5 or more could be observed.

Like Cassini et al.(2001), when we studied the effect of undershooting and microscopic diffusion, we observed a change in the luminosity at which the bump occurred but no change in the slope of the discontinuity when these parameters are taken into account.
Even if the shape is not quite the same, we can compare the case of the artificial smoothing added in the article to our case of turbulent diffusion where the discontinuity is also smoothed. We saw that this had the effect of making the decrease in luminosity less significant. As explained in section 5.6, when the bump is smaller, the impact on observations would be that more stars would be found in a reduced luminosity interval. We therefore have the same type of result as Cassisi et al.(2001) and their luminosity functions are consistent with what we would expect from our results.
Finally, they didn't observe any change of shape when they changed the opacity at the discontinuity. We did not look at a direct change in opacity, but we looked at changes in metallicity that lead to a change in opacity. Although the luminosity at which the bump occurs changes, we don't see a change in the size of the bump, so we would effectively see no difference in the shape of a luminosity function.

6.2 "The magnitude difference between the main sequence turn off and the red giant branch bump in Galactic globular clusters" (Cassisi et al., 2011)

The second paper by Cassisi et al. (2011) aims to present new magnitude measurements for the main sequence turn-off (TO) and for the bump. Using the filter F606W, for their observations, they determine the apparent magnitude of the TO and of the bump and use the relative distance of the clusters from the MS-fitting technique. They then determine the age of the clusters from the absolute magnitude of the TO. It was for this purpose that they selected the clusters to be studied. Some were too bright, and thus saturated the image, other clusters had too few stars in the RGB phase, the bump was therefore undetectable (these are mostly those with low metallicity). Then

another selection criterion was that their metallicity had recently been re-estimated. In the end twelve clusters covering a wide range of metallicity were selected.

To determine the magnitude of the bump, they count the number of stars as a function of brightness and make a linear fit that represents the continuum. They then subtract this continuum and look at the maximum.

They made models for M_{F606W}^{TO} and $\Delta M_{F606W}^{TO-Bump}$, which are respectively the magnitude of the turn-off and the difference of luminosity between the turn-off and the bump in the F606W filter, as a function of the metallicity [M/H] for several cluster ages. They observe that the bump is more tenuous with age and $\Delta M_{F606W}^{TO-Bump}$ increases. By setting the points for the measured clusters, they found that the age obtained by $\Delta M_{F606W}^{TO-Bump}$ is smaller than that obtained by the TO, i.e. the bump would be too bright. The discrepancy between observations and theory does not change with metallicity, the error being always approximately 0.2 mag.

Several hypotheses are put forward to explain this. The first is that the values of [M/H] are underestimated but there is no indication that this would be the case. The second, that opacity would be underestimated but they found this unlikely. It is also suggested that this could be due to the lack of consideration of atomic diffusion but even if this were taken into account it would be inhibited by turbulence and would not reduce the discrepancy sufficiently compared to other factors not taken into account which would increase it. A last solution would be to introduce undershooting.

The method for studying the bump in this second paper by Cassisi et al. (2011) is very different from what we have done here. It is therefore difficult to compare what they did with what has been done here. Nevertheless we can note that their final conclusion was that the bump in their models occurs at too high luminosity compared to the observations. They put forward several hypotheses to explain this. Among the least likely they propose that metallicity has been underestimated. We studied the effect of metallicity and saw that if metallicity was underestimated, then the bump in the model would be brighter than with higher metallicity. So even though it is unlikely, this explanation could explain the discrepancy. A second hypothesis is the introduction of microscopic diffusion and we have seen that indeed taking this

into account would reduce the luminosity they would obtain for their models. However, it is true that the effect is not very pronounced and would probably not solve the discrepancy by itself. Finally, for the favored hypothesis which is the introduction of undershooting in the models, we have also studied this parameter and we have seen that indeed the introduction of undershooting in the models allows to obtain a bump which occurs at lower luminosity and the effect is more pronounced than for the introduction of microscopic diffusion. This could therefore be the source of the discrepancy between their models and observations.

6.3 "The Red-Giant Branch Bump Revisited: Constraints on Envelope Overshooting in a Wide Range of Masses and Metallicities" (Kahn et al., 2018)

The third paper, by Khan et al. (2018), analyses the bump using a combination of asteroseismology and spectroscopy. With this method they can study a data set of nearly 3000 red-giant stars independently of distance and with wide ranges of mass, age and metallicity.

The masses studied range from 1.0 to 1.6 $M_{\odot}$ and [M/H] from -0.4 to 0.2 dex. Undershooting is studied for efficiency values of 0.0 (thus no undershooting), 0.025 and 0.05, corresponding to undershooting parameters of $\alpha = 0$, $\alpha = 0.3$ and $\alpha = 0.6$ respectively.

They compare the observed data with those obtained in simulations by plotting graphs representing the seismic parameter ν_{max} as a function of temperature. $1/\nu_{max}$ can be used as a proxy for the luminosity. By assembling the data into several mass and metallicity intervals, they determined the location of the bump and compared the change in the bump caused by changing these parameters. The seismic parameter of the bump decreases with increasing mass and decreasing metallicity. So a larger mass leads to a higher luminosity and a higher metallicity leads to a lower luminosity.

When undershooting is not taken into account, there is a discrepancy between observation and models, the models give values of the bump that are too bright. The next objective is then to compare the observation with

various models using different undershooting parameters. Thus for each observation a value of the undershooting parameter can be found to compensate for the discrepancy. Indeed the undershooting will lower the luminosity at which the bump occurs. A more important undershooting seems to be necessary in the case of metal-poor stars. However, the undershooting parameter never exceeds 0.6.

Uncertainties other than that of the undershooting parameter exist. In addition to the parameters already mentioned, initial helium abundance and overshooting have been studied. By increasing the initial helium abundance, they find that the bump occurs at higher luminosity. By adding overshooting, they find that the presence of this last has no impact on the bump.

A combination of several changes in the parameters can lead to a disappearance of the discrepancy but the preferred parameter to explain the discrepancy is the undershooting which must be taken into account.

As in the previous article, the method used differs a lot from ours. Nevertheless, we can compare their conclusions on the impact of the parameters on luminosity with what we have obtained.

The first result they show is that the luminosity of the bump increases with increasing mass and decreasing metallicity, which we also obtained.

As proposed in the previous article they use undershooting to make the discrepancy disappear. So they have that the undershooting lowers the bump luminosity as we obtained for our models.

Concerning the overshooting, they don't get any impact. We have seen in our study of overshooting that it can have a very big impact on the bump but that indeed, depending on the mass of the star and the overshooting parameter, the effect can also be minor. It is therefore possible that for the parameters they have chosen, overshooting is negligible. But it cannot be neglected in a general way in the study of the bump.

7 Conclusion

In order to better understand the red giants branch bump, we have tried to understand the influence of several parameters on it with the help of the stellar evolution code Clés. Several models has thus been implemented by modifying the total mass of the star, its overshooting and undershooting parameters, its metallicity and by looking at cases with or without microscopic and turbulent diffusion. From these models, mainly by looking at their HR plot and hydrogen abundance profile, the changes caused on the bump have been identified and it has been explained why they occurred.

For the total mass of the star, it has been observed that the luminosity at which the bump occurs increases with the mass. This is due to the fact that for a star of greater mass, it has a more massive core when the discontinuity is reached by the H-burning shell. As for the importance of the luminosity decrease, no direct relation has been observed.

Overshooting alters what happens during the main sequence. This leads to a different hydrogen profile at the base of the red giant branch. This change in the profile can have a very big impact on the bump (1.8 $M_\odot$) as well as in some cases only a minor impact (1.3 $M_\odot$). In general it will lead to a greater luminosity for the beginning of the bump but the size of the bump can be larger (1.8 $M_\odot$) or smaller (1.3 $M_\odot$) depending on the considered case. The presence of overshooting can even make the bump disappear for a star of sufficient mass as shown for a star of 2.2 $M_\odot$.

Undershooting causes the convective envelope to descend further into the star. The higher the undershooting parameter is set, the earlier the H-burning shell reaches the discontinuity, and therefore, with a lower core mass. The bump thus occurs at lower luminosity when the undershooting parameter is higher.

For metallicity, the luminosity at which the bump occurs is lower for a higher metallicity. This can be explained by the fact that, when there is a higher metallicity, on the one hand the discontinuity is deeper in the star and on the other hand the core of the star is smaller. The size of the discontinuity in the hydrogen profile is not impacted, which means that the luminosity drop is the same for each metallicity studied.

Finally, two cases of diffusion were studied, microscopic diffusion and turbulent diffusion.

In the first case, the presence of microscopic diffusion leads to a disconti-

nuity located deeper in the star, so the bump occurs at lower luminosity but the difference with the case without microscopic diffusion is quite small.

In the presence of turbulent diffusion, in addition to the fact that the discontinuity is located less deep in the star, it is also softer which leads to a lesser reduction in luminosity during the bump.

When analyzing the various parameters for their effects on the bump, attention has been focused mainly on what happens to the luminosity at which the bump occurs and the resulting decrease in luminosity. As briefly mentioned in section 5.6, the duration of the bump could also have an impact on the observation of the bump and would therefore be an interesting factor to analyze in order to go further in this study.

All these results were then compared to three articles about the bump. Although the methods were not the same, the results tend to be the same when a comparison is possible.

Another interesting way to go further in the study of the bump would be to establish luminosity functions as was done in the first paper, presented by Cassisi et al. (2001), or even better, to be able to obtain cluster observations to compare the observations with our models. We could then try to better calibrate the different parameters composing the star. One could also explore other values of the parameters studied above or try to understand the influence of other parameters, for example the initial helium abundance cited by Khan et al. (2018) but not explored at all here.

Bibliography

Adelberger, E. G., Garcia, A., Robertson, R. G. H., Snover, K. A., Balantekin, A. B., Heeger, K., et al. (2011). Solar fusion cross sections. II. The pp chain and CNO cycles. Reviews of Modern Physics 83, 195–246. doi:10.1103/RevModPhys.83.195

Asplund, M., Grevesse, N., Jacques Sauval, A., Scott, P. (2009). The chemical composition of the Sun, arXiv:0909.0948

Bjork, S. R. and Chaboyer, B., Theoretical Uncertainties in Red Giant Branch Evolution: The Red Giant Branch Bump, (2005). arXiv:astro-ph/0512508

Bossini, D., Miglio, A., Salaris, M., Girardi, L., Montalbàn, J., Bressan, A., Marigo, P. and Noels, A., (2015). The AGB bump: a calibrator for core mixing, arXiv:1502.03318

Cassisi, S., Salaris, M., Bono, G, (2001). The shape of the Red Giant Branch Bump as a diagnostic of partial mixing processes in low-mass stars, arXiv:astro-ph/0110247

Cassisi, S., Marín-Franch, A., Salaris, M., Aparicio, A., Monelli, M. and Pietrinferni, A., (2011). The magnitude difference between the main sequence turn off and the red giant branch bump in Galactic globular clusters AA 527, A59

Dupret, M.-A., Stellar structure and evolution I & II

Iben, I., (1968). 220, 143, Age and Initial Helium Abundance of Stars in the Globular Cluster M15, Nature, doi: 10.1038/220143a0

Irwin, A. W. (2012). FreeEOS: Equation of State for stellar interiors calculations. Astrophysics Source Code Library

Jorissen, A., (2016). Astrophysique PHYS-F-438

Joyce, M., Chaboyer, B., (2015). Investigating the Consistency of Stellar Evolution Models with Globular Cluster Observations via the Red Giant Branch Bump, arXiv:1510.07648

Khan, S., Hall, O., J., Miglio, A., Davies, G., R., Mosser, B., Girardi, L., and Montalbàn, J., (2018). The Red-Giant Branch Bump Revisited: Constraints on Envelope Overshooting in a Wide Range of Masses and Metallicities, arXiv:1804.06669v1

King, C., R., Da Costa, G. S., Demarque, P., (1985). The luminosity function on the subgiant branch of 47 Tucanae : a comparison of observation and theory., ApJ, 299, 674, doi: 10.1086/163733

Lagioia, E., P., Milone, A., P., Marino, A., F, Cassisi,S., Aparicio, A., J.,

Piotto, G., Anderson, J., Barbuy, B., Bedin, L., R., Bellini, A., Brown, T., D'Antona, F., Nardiello, D., Ortolani, S.,Pietrinferni, A., Renzini, A., Salaris, M., Sarajedini, A., van der Marel, R. and Vesperini, E., (2018). The Hubble Space Telescope UV Legacy Survey of Galactic Globular Clusters – XII. The RGB bumps of multiple stellar populations, doi:10.1093/mnras/sty083

Nataf, D., M., (2014). Red giant branch bump star counts in data and stellar models, doi:10.1093/mnras/stu1974

Noels, A., The Golden Gift of Red Giants

Rogers, F., J., Swenson, F. J., and Iglesias, C. A. (1996). OPAL Equation-of-State Tables for Astrophysical Applications. ApJ 456, 902. doi:10.1086/176705

Scuflaire, R., Théado, S., Montalbàn, J., Miglio, A., Bourge, P.-O., Godart, M., Thoul, A., Noels A., (2007). CLÉS, Code Liégeois d'Évolution Stellaire, arXiv:0712.3471

Thomas, H.-C. (1967). ZA, 67, 420